Historical Biology

An International Journal of Paleobiology

ISSN: (Print) (Online) Journal homepage: https://www.tandfonline.com/loi/ghbi20

Redescription of the dorsal vertebrae of the mamenchisaurid sauropod *Xinjiangtitan shanshanesis* Wu et al. 2013

Xiao-Qin Zhang, Ning Li, Yan Xie, Da-Qing Li & Hai-Lu You

To cite this article: Xiao-Qin Zhang, Ning Li, Yan Xie, Da-Qing Li & Hai-Lu You (2022): Redescription of the dorsal vertebrae of the mamenchisaurid sauropod *Xinjiangtitan shanshanesis* Wu et al. 2013, Historical Biology, DOI: 10.1080/08912963.2022.2147428

To link to this article: https://doi.org/10.1080/08912963.2022.2147428

Published online: 08 Dec 2022.

HISTORICAL BIOLOGY
https://doi.org/10.1080/08912963.2022.2147428

Taylor & Francis
Taylor & Francis Group

Redescription of the dorsal vertebrae of the mamenchisaurid sauropod *Xinjiangtitan shanshanesis* Wu et al. 2013

Xiao-Qin Zhang[a], Ning Li[b], Yan Xie[c], Da-Qing Li[b,d] and Hai-Lu You[e,f,g]

[a]Gansu Geological Museum, Lanzhou, P. R. China; [b]School of Earth Sciences and Resources, China University of Geosciences (Beijing), Beijing, P. R. China; [c]Turpan Bureau of Natural Resources, Turpan, Xinjiang; [d]Institute of Vertebrate Paleontology and College of Life Science and Technology, Gansu Agricultural University, Lanzhou, P. R. China; [e]Key Laboratory of Vertebrate Evolution and Human Origins of Chinese Academy of Sciences, Institute of Vertebrate Paleontology and Paleoanthropology, Chinese Academy of Sciences, 142 Xizhimenwai Street, Beijing 100044, P. R. China; [f]CAS Center for Excellence in Life and Paleoenvironment, Beijing, P. R. China; [g]College of Earth and Planetary Sciences, University of Chinese Academy of Sciences, Beijing, P. R. China

ABSTRACT

The dorsal vertebrae of *Xinjiangtitan shanshanesis* (SSV12001) from the Late Jurassic Qigu Formation of Xinjiang Uygur Autonomous Region, China, are redescribed based on the further exposure and preparation of the holotype. As a mamenchisaurid sauropod dinosaur, *Xinjiangtitan shanshanesis* displays a unique combination of autapomorphic and plesiomorphic features, such as the presences of both lateral spinopostzygapophyseal laminae (L.SPOL) and medial spinopostzygapophyseal lamina (M.SPOL) in dorsal vertebrae and a shallow intralaminar fossa (SPOL-F) between the L.SPOL and M.SPOL; anterior spinodiapophyseal laminae (A.SPDL), posterior spinodiapophyseal laminae (P.SPDL) and middle spinodiapophyseal lamina (M.SPDL) in dorsals 3–5; bifurcated anterior and middle dorsal neural spines with the median tubercle and the triangular lateral processes. Phylogenetic analysis and morphological comparison show that *Xinjiangtitan shanshanesis* probably shares a close relationship with *Hudiesaurus* and *Mamenchisaurus* and provide new information for future taxonomic revision of the mamenchisaurids.

ARTICLE HISTORY
Received 25 July 2022
Revised 10 November 2022
Accepted 10 Nov 2022

KEYWORDS
Xinjiangtitan shanshanesis; dorsal vertebrae; late Jurassic; Qigu Formation; Xinjiang

Introduction

The characteristics associated with vertebrae are critical in sauropod studies (Harris 2006a, 2006b), and their morphology is of primary importance in understanding sauropod phylogeny and evolution (Bonaparte 1986; Alexander 1989; Martin et al. 1998; Seymour and Lillywhite 2000; Wilson 2002). The terrestrial Middle and Late Jurassic strata in China are rich in mamenchisaurid fossils, and the axial skeletons of some of these sauropods are preserved completely (e.g. *Mamenchisaurus youngi* Ouyang and Ye 2002; *Mamenchisaurus hochuanensis* Young and Chao 1972). The anatomies of these taxa are important to clarify the evolutionary interrelationships of these and related Middle-Late Jurassic taxa.

Wu et al. (2013) briefly described a new mamenchisaurid sauropod *Xinjiangtitan shanshanesis* from the Late Jurassic Qigu Formation based on field observation. Following this, the complete and articulated vertebral column was exposed from further excavation in 2014 and 2015. This discovery sheds light on the restudy of this taxon and the evolution of mamenchisaurid sauropods. The primary anatomical information remains a central pillar of dinosaur palaeobiology (Hedrick and Dodson 2020), and redescription of the historically and taxonomically important mamenchisaurid specimens is much needed in broader morphofunctional and palaeobiogeographical research (Moore et al. 2020). Zhang et al. (2020) restudied the complete cervical vertebrae of this taxon. Here, we further redescribe and illustrate the complete dorsal vertebral column of *Xinjiangtitan shanshanesis* and revise its unique characteristics. We also morphologically compared *Xinjiangtitan shanshanesis* to other mamenchisaurid and relevant sauropods from the Middle-Late Jurassic and Early Cretaceous of China and performed a cladistic analysis with this new information.

Systematic palaeontology

Dinosauria Owen 1842

Saurischia Seeley 1887

Sauropodomorpha Huene 1932

Sauropoda Marsh 1878

Eusauropoda Upchurch 1995

Mamenchisauridae Young and Chao 1972

Xinjiangtitan Wu et al. 2013

Xinjiangtitan shanshanesis Wu et al. 2013

Holotype

Xinjiangtitan shanshanesis (SSV12001) includes a complete axial skeleton and pelvic girdle and hind limb, as shown in Zhang et al. (2020).

Occurrence and horizon

According to Wu et al. (2013), *Xinjiangtitan shanshanesis* (SSV12001) was excavated from the quarry 8 km south to Qiketai, 30 km east to Shanshan. The horizon was from the brown – red, grey – green argillaceous siltstone at the middle beds of the Qigu Formation. The lower part of the Qigu Formation has been dated 151 Ma, and the Jurassic-Cretaceous boundary is located in the upper part of the Qigu Formation (Fang et al. 2015; Huang 2019), suggesting that *Xinjiangtitan shanshanesis* is from the Late Jurassic.

CONTACT Xiao-Qin Zhang cici___pig1@163.com; Gansu Geological Museum, 6 Tuanjie Road, Lanzhou 730030, P. R. China

Published online 08 Dec 2022

Revised Diagnosis of dorsal vertebrae

The dorsal vertebrae of *Xinjiangtitan shanshanesis* are distinguished from other known mamenchisaurid sauropods by the following unique combination of character states (characters with an asterisk represent autapomorphies of *Xinjiangtitan shanshanesis*): (1) presence of both lateral spinopostzygapophyseal lamina (L. SPOL) and medial spinopostzygapophyseal lamina (M.SPOL) and a shallow intralaminar spinopostzygapophyseal lamina fossa (SPOL-F) inbetween in dorsals 3–11; (2) pits on dorsal surface of prezygapophyses in last cervical and dorsals 1–2(similar to *Hudiesaurus sinojapanorum*); (3) hyposphene- hypantrum system in dorsals 3–7, with the 'Y'-shaped hypantrum in dorsal 4 and a single vertical hypantrum in dorsal 7*; (4) a subtle keel subdividing spinodiapophyseal fossa in dorsals 1–2 (similar to *Klamelisaurus gobiensis*); (5) anterior spinodiapophyseal lamina (A.SPDL), posterior spinodiapophyseal lamina (P.SPDL) and middle spinodiapophyseal lamina (M.SPDL) in dorsals 3–5*; (6) dorsally bifurcated middle spinodiapophyseal lamina (M.SPDL) in dorsals 4–5 (similar to *Klamelisaurus gobiensis*); (7) neural spine bifurcated with the median tubercle and triangular lateral processes in anterior and middle dorsal vertebrae; (8) sloping secondary crests situated at the dorsal end of the spinodiapophyseal fossa (SDF) in middle dorsal vertebrae*; (9) dorsally bifurcated spinoprezygapophyseal lamina (SPRL) in some middle dorsals*; (10) bipartite or triplicate PCPLs in some middle-posterior dorsal vertebrae (similar to *Klamelisaurus gobiensis*); (11) two nearly parallel centropostzygapophyseal laminae (CPOLs) in posterior dorsal vertebrae*.

Description

The following description is based on the complete elements (Figure 1). Osteological descriptions are organised as anatomical subdivisions (Dorsal vertebrae and Dorsal ribs). See Table 1 for measurements of dorsal vertebrae.

Dorsal vertebrae

Xinjiangtitan shanshanesis (SSV12001) includes a complete, articulated dorsal series extending from dorsal 1 to dorsal 12. The dorsal series are generally in excellent condition, but there are minor damages in several parts. The lower portions of centra of dorsals 1–8, the dorsal portion of neural arch and neural spine of dorsal 12 are missing. All dorsal vertebrae show strongly opisthocoelous with

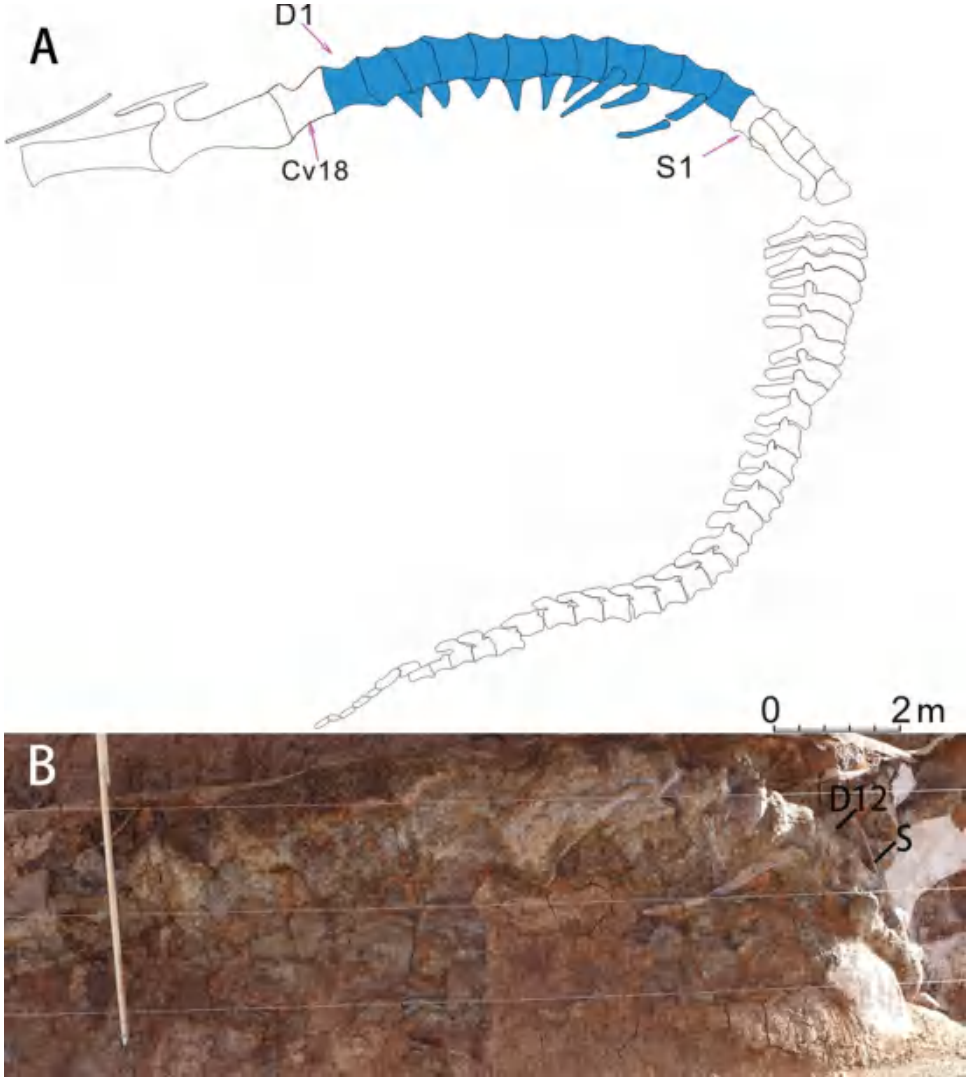

Figure 1. Preserved dorsal elements of *Xinjiangtitan shanshanesis* (SSV12001). A, burial condition of dorsal elements of SSV12001; B, field photograph of dorsal elements of SSV12001.

Table 1. Dorsal vertebral measurements of *Xinjiangtitan shanshanesis* (SSV12001) (in mm).

Vert	Max centr length	Min centr length	Pa width	Max Vert Ht	T.P width	Pneu Foss Ht	Pneu Foss length	Anter Artc Ht	Anter Artc width	Poster Artc Ht	Poster Artc width	Pre Zyg width	Post Zyg width	Neural Arch Ht ±	Spin Proc Ht 1	Spin Proc Ht 2	Spin Proc Max Med-Lat Width 3	Spin Proc Max Anter Poster length
D1	– –	310	70	740	370*	170	200	– –	– –	– –	430	100	130	210-	290	460	170,450	260#
D2	330	290	70	– –	370	– –	– –	– –	400	– –	– –	200	200	– –	245	495	160,470	200#
D3	– –	240*	70	– –	370	– –	– –	– –	– –	– –	– –	– –	170	230-	160*	470	350	160#
D4	370	270	70	– –	270	70	130	– –	– –	– –	– –	140	– –	200+	150	400	350	90#
D5	– –	290	70	– –	240	– –	– –	– –	– –	– –	– –	– –	– –	– –	170	460	340	60#
D6	– –	280	– –	– –	240	– –	– –	– –	– –	– –	– –	– –	120	270-	140	480	330	45#
D7	340	260*	70	920	210	100	130	370	370	– –	– –	90	– –	300+	230	500	340	70
D8	– –	260	70	940	180	110	150	– –	– –	– –	– –	– –	– –	– –	210	510	330	80
D9	– –	230	70	990	160	80	140	– –	– –	380	410	– –	110	340-	230	590	320	100
D10	240*	190*	– –	1030	200	110	110	450	350	220*	– –	110	– –	220+	280	580	200*	85*
D11	– –	200*	50	1040	150	120	90	210*	– –	385*	400	– –	120	250-	300	590	200*	80*
D12	320	220	40	– –	– –	80	110	400	400	440	445	100	– –	230+	– –	– –	– –	– –

Note: Pa Width, measured the distance of the mediolateral width of the parapophysis; T.P Width, measured the distance of the mediolateral width of the transverse process *measured distance based on diagenetically distortion; – – distance not be accurately measured or unsaved; Pre Zyg Width, the distance of prezygapophysis anteroposteriorly; Neural Arch Ht+, measured from the ventral margin of neural canal to the ventral margin of prezygapophyses; Neural Arch Ht-, measured from the ventral margin of neural canal to the ventral margin of postzygapophyses; 1: measured from anterioralmost point on spinoprezygapophyseal lamina; 2: measured from dorsal margin of neural foramen on the posterior end; 3, if two values given, first, distance between paired metapophyses, second, distance between two triangle lateral processes; #, the length of bifurcation anteroposteriorly.

deep pleurocoels located at the most anterolateral portion of the centra. Pneumaticity extends throughout the centrum and the neural arch. The lamination is well developed in dorsal series. There is some distance between the postzygapophyses on both sides in dorsal 1, but the postzygapophyses are adjacent to each other in dorsals 3–12. And that, the hyposphene-hypantrum system appears from dorsal 3 to subsequent dorsals as in most sauropods (Upchurch et al. 2004). Neural spines are all bifurcated except for the last three dorsal vertebrae.

The 18th vertebra was recognised as the first dorsal vertebra, and the 10th and the11th dorsal vertebrae were identified as a single dorsal vertebra by Wu et al. (2013). By reobservation and redescription, the centrum of the 19th vertebra is regarded as the first dorsal vertebra, because the less elongated antero-posteriorly centrum (the minimum centrum length 310 mm is less than half of the 17th centrum 730 mm) with the typical undivided pleurocoel, and its stouter transverse process projects more horizontally than previous vertebra, as suggested by Zhang et al. (2020).

We divide the description into sections of dorsal vertebrae 1–3, dorsal vertebrae 4–9, dorsal vertebrae 10–12 based on morphology and condition of articulation.

Dorsal vertebrae 1-3

Dorsal 1

The cervicodorsal transition here is continuous. The first dorsal vertebra identified here was preserved articulated with the last cervical vertebra. The lower portion of dorsal 1 is not preserved (parapophyses are missing) and reconstructed by plaster (Figure 2).

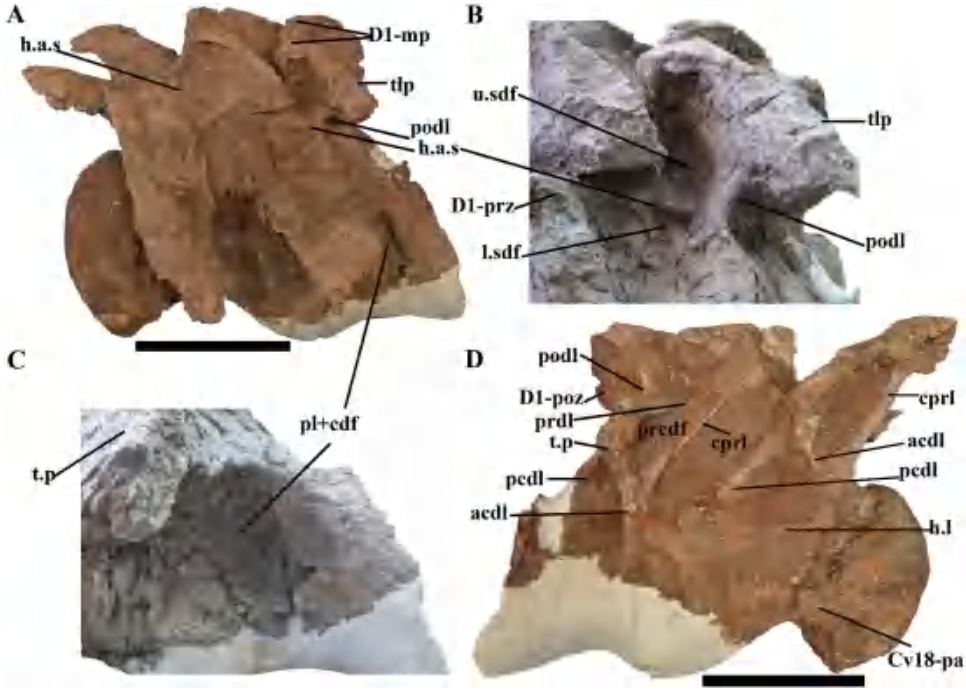

Figure 2. Photographs of cervical 18 and dorsal 1 of *Xinjiangtitan shanshanesis* (SSV12001). A, left lateral view; B, close-up of left lateral view of the horizontal accessory strut of dorsal1; C, close-up of left lateral view of pleurocoel; D, right lateral view. Scale bars: A, D, 30 cm; B, C, not to scale.

The centrum is longer anteroposteriorly than that of the following dorsal vertebrae but shorter than those of the preceding cervical vertebrae. The centrum is strongly opisthocoelous, and the depth of the cotyle is about one-third of the minimum length of centrum (exclude the condyle length) (Figure 2). In the left lateral view, the single and large pleurocoel deepens to invade the condyle anteriorly, which dorsally merges with the centrodiapophyseal fossa (CDF) (Figure 2 A, 2C). In the right lateral view, the anteroventrally orientated anterior centrodiapophyseal lamina (ACDL) and the comparatively strong posterior centrodiapophyseal lamina (PCDL) bound a deep centrodiapophyseal fossa (CDF) just below the base of the transverse process.

The height of the neural arch (measured as the distance from the dorsal margin of the centrum to the level of the base of the postzygapophyses) is relatively lower than that of the succeeding dorsals. The transverse processes present as plate-like processes, projecting more horizontally than that of cervical 18 (Figure 2A,). The prezygapophyses of dorsal 1 are articulated with the postzygapophyses of cervical 18. The centroprezygapophyseal lamina (CPRL) extends ventrally to meet the anterodorsal part of the ACDL. The prezygodiapophyseal lamina (PRDL) extends anterodorsally from the transverse process to the prezygapophysis at 20° to the horizontal, whereas the postzygodiapophyseal lamina (PODL) is nearly vertically projected (Figure 2B, 2D). The PRDL, the ACDL and the CPRL outline an anterodorsally to posteroventrally elongated triangular prezygapophyseal centrodiapophyseal fossa (PRCDF) on the neural arch (Figure 2D). The postzygapophyses protrude ventrolaterally, and the postzygapophyseal facets are much transversely wider than the anteroposterior length. In the right lateral view, the postzygodiapophyseal lamina (PODL) extends from the dorsolateral margin of the transverse process to the postzygapophysis. In posterior view, the two almost parallel centropostzygapophyseal laminae (CPOLs) support the postzygapophyses. The medial margins of the postzygapophyses descend slightly medially and merge to form an incipiently developed 'V' -shaped intrapostzygapophyseal laminae (TPOLs) (Figure 2C).

The neural spine bifurcates with a median tubercle and two metapophyses (Hatcher 1901; Wiman 1929; Gilmore 1936; Harris 2006a; Zhang et al. 2020) as that in cervical 18. The median tubercle is lower than the metapophyses and slightly expanded posteriorly, thereinto, a developed notch between the median tubercle (Hatcher 1901; Wiman 1929; Gilmore 1936; Harris 2006b) and each of the paired metapophyses. The paired metapophyses correspond to the 'processus pseudospinosus', as suggested by Wilson and Upchurch (2009) and Wiman (1929). Each metapophysis extends posterolaterally to develop a triangular lateral process (TLP), which overlaps the dorsal surface of postzygapophysis, respectively, merging with the spinopostzygapophyseal lamina (SPOL). In contrast to the bifurcation of the neural spine in cervical 18, the median tubercle of dorsal 1 is very developed in dorsal view, while the metapophysis extends more laterally than posteriorly as a flat broad lamina, and the end of which no longer expands laterally as a prominent triangular precess as that of cervical 18. Thus, the neural spine becomes 'trifid', which is similar to that in *Hudiesaurus* (Dong 1997), *Klamelisaurus gobiensis* (Zhao 1993; Moore et al. 2020) and *Euhelopus zdanskyi* (Wilson and Upchurch 2009). However, the bifurcation area of *Xinjiangtitan* presents as a 'W'-shaped cleft in dorsal view and becomes'U'-shaped in posterior view (Figure 2A, 2B; Figure 3A, 3B, 3C). We will compare these groups in detail in the following paragraphs. Laterally, as in the cervical series, the first dorsal vertebra lacks the spinodiapophyseal lamina (SPDL) which is replaced by a horizontal accessory strut (H.A.S) connecting the medial margin of prezygapophysis and the base of the postzygodiapophyseal lamina (PODL). The horizontal accessory strut subdivides the spinodiapophyseal fossa (SDF) into an upper spinodiapophyseal fossa (U.SDF) and a lower one (L.SDF) on the base of spine of dorsal 1 (Figure 2A, 2B). Furthermore, this condition is also present in cervicals of *Euhelopus zdanskyi* (PMU 233; Wilson and Upchurch 2009: Figs. 9, 10, 12) and resembles the posterior continuation of the pre-epipophysis of cervicals 10-16 in *Klamelisaurus gobiensis* (Moore et al. 2020: Figs. 3–6). It suggests that the first dorsal vertebra is probably a functional cervicodorsal vertebra, which has more osteological mobility than that of the following dorsal vertebrae (Vidal et al. 2020).

Dorsals 2-3

These two dorsal vertebrae are preserved in articulation with each other. The lower parts of centra are not preserved and are rebuilt with plaster. The remains of the centra are typically opisthocoelous with a well-developed anterior condyle and corresponding posterior cotyle. The centrum of dorsal 3 shortens anteroposteriorly relative to dorsal 2. Only the left parapophyses of dorsals 2–3 are preserved as laterally directed processes and position in the dorsal portions of the centra (Figure 4).

In the left lateral view, the plate-like transverse processes project horizontally but the ends of transverse processes projecting ventrally with gently concave articular surfaces for ribs. The transverse processes of dorsal 2 position in the dorsal portion of the neural arch just below the level of the prezygapophyses, while the

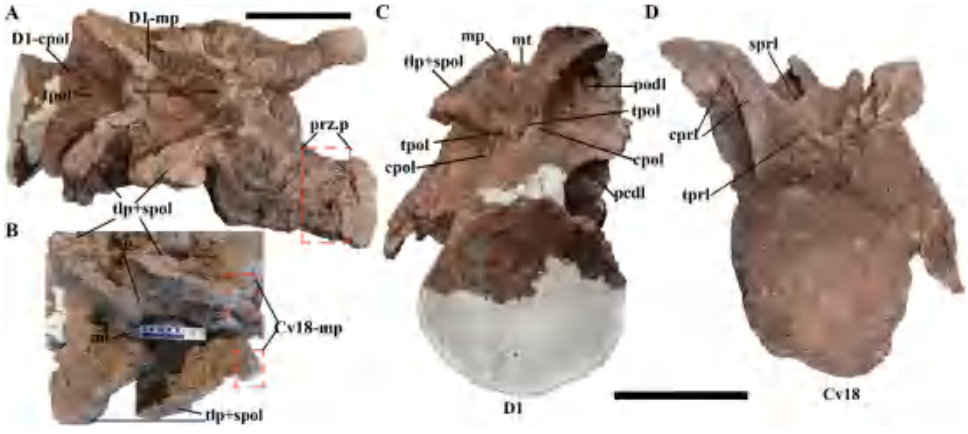

Figure 3. Photographs of cervical 18 and dorsal 1 of *Xinjiangtitan shanshanesis* (SSV12001) in dorsal, posterior and anterior views. A, dorsal view; B, close-up of dorsal view of neural spine; C, posterior view; D anterior view. Scale bar: A, C, D, 30 cm; B, 10 cm.

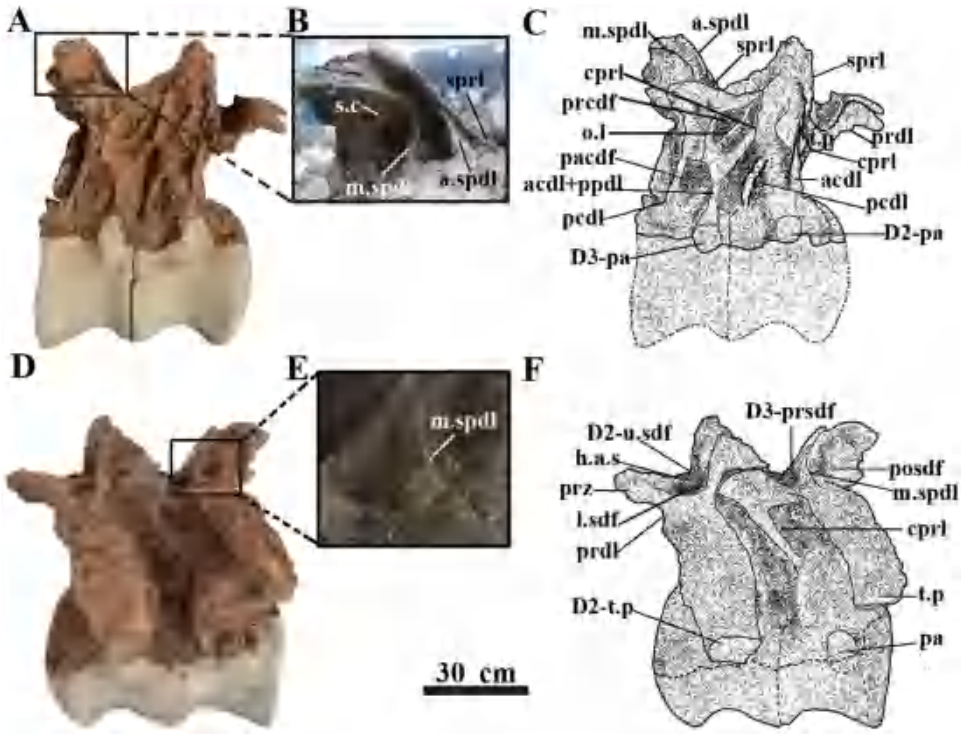

Figure 4. Dorsal vertebrae 2–3 of *Xinjiangtitan shanshanesis* (SSV12001) in lateral views. A, right lateral view; B, close-up of right spinodiapophyseal fossa of dorsal 3; C, schematic of right lateral view; D, left lateral view; E, close-up of left spinodiapophyseal fossa of dorsal 3; F, schematic of left lateral view. Scale bars: A, C, D, F, 30 cm; B, E, not to scale.

transverse processes of dorsal 3 ascend up to the level of prezygapophyses. In the right lateral view, the transverse processes of dorsals 2–3 are broken, only the bases of transverse processes are preserved and migrate to the anterior portion of the neural arch (Figure 4A, 4C). In dorsal 2, the short PRDL projects anterodorsally to meet the lateral margin of the prezygapophysis as in dorsal 1. The partial CPRL extends posteroventrally from the ventral aspect of the prezygapophysis to the neural arch in the right lateral view of dorsal 2, which is a broad flat sheet beneath the prezygapophysis in anterior view (Figure 5A, 5B, 5C ,). The ACDL extends from the posteroventral margin of the transverse process down to the anterolateral section of the centrum (Figure 4A, 4C), whereas the PCDL is broken and only the lower portion is preserved. By contrast, the laminae and fossae could be prominently observed in dorsal 3. The paradiapophyseal lamina (PPDL) originates from the base of the transverse process to connect the parapophysis on the neurocentral junction, which merges with the ACDL (Figure 4A, 4C). Furthermore, the PPDL+ACDL and PCDL bound a broad triangular parapophyseal centrodiapophyseal fossa (PACDF) on the neural arch. The CPRL in dorsal 3 is a variant that is canted anteriorly and contacts the PPDL+ACDL ventrally rather than the anterior margin of neurocentral junction. The CPRL, the PRDL, the transverse process and the partical ACDL + PPDL bound a well-defined prezygapophyseal centrodiapophyseal fossa (PRCDF) subdivided by an oblique lamina (O.l) (Figure 4A, 4C), which is corresponding to 'cranial infradiapophyseal fossa' suggested by Harris (Harris 2006a).

In left lateral view, there is a deep dorsoventrally elongated SDF on the base of the neural spine of dorsal 2, which is also divided into U.SDF and L.SDF by the horizontal accessory strut as that in dorsal 1 and posterior cervicals (Figures 2A, 2D, 4F). However, the SDF of dorsal 3 presents as an anteroposteriorly elongated deep fossa, which is divided into an anterior prezygapophyseal spinodiapophyseal fossa (PRSDF) and a posterior postzygapophyseal spinodiapophyseal fossa (POSDF), respectively, by the middle spinodiapophyseal laminae (M. SPDL) (Figure 4). The M. SPDL appears as an anteriorly bended ridge on the midline of the proximalmost part of the transverse process. In addition to the M. SPDL, there are anterior spinodiapophyseal laminae (A. SPDL) extending from the anterior margin of the transverse process to merge with the SPRL and a short sloping secondary crest (S.C) in the end of the SDF (Figure 4A, 4B).

In anterior view, the dorsomedially oriented prezygapophyses of dorsal 2 meet each other via a horizontal lamina (H.L), the position of which is equivalent to that of the TPRL, but it is difficult to confirm if this lamina is the TPRL because of the unrepaired neural canal (Figure 5A, 5C). Dorsally, the articular surfaces of the prezygapophyses are prominently extended transversely and convex dorsally though they are not well preserved. There are also some small coels on the dorsal surface of the left prezygapophysis as those on cervical 18 (Figures 3 A; 6A), this condition resembles the pits on the dorsal surface of prezygapophysis (PRZ.P) of *Hudiesaurus sinojapanorum* (Upchurch et al. 2021: Fig. 3). In posterior view, the postzygapophyses of dorsal 3 are adjacent to each other without TPOL, and their articular facets are gently concave. The ventrally oriented hyposphene extends from the base of the postzygapophyses connection to the top of the neural canal in dorsal 3 so as to strengthen the union between adjoining vertebrae (Figure 5). A pair of lateral spinopostzygapophyseal laminae (L. SPOL) connects the dorsolateral parts of postzygapophyses to the top of the neural spine of dorsal 3 respectively. Furthermore, a pair of stout ridges originates from the dorsomedial parts of postzygapophyses near the midline of the postzygapophyses to meet the median tubercle of the neural spine. Here, we define them as the medial

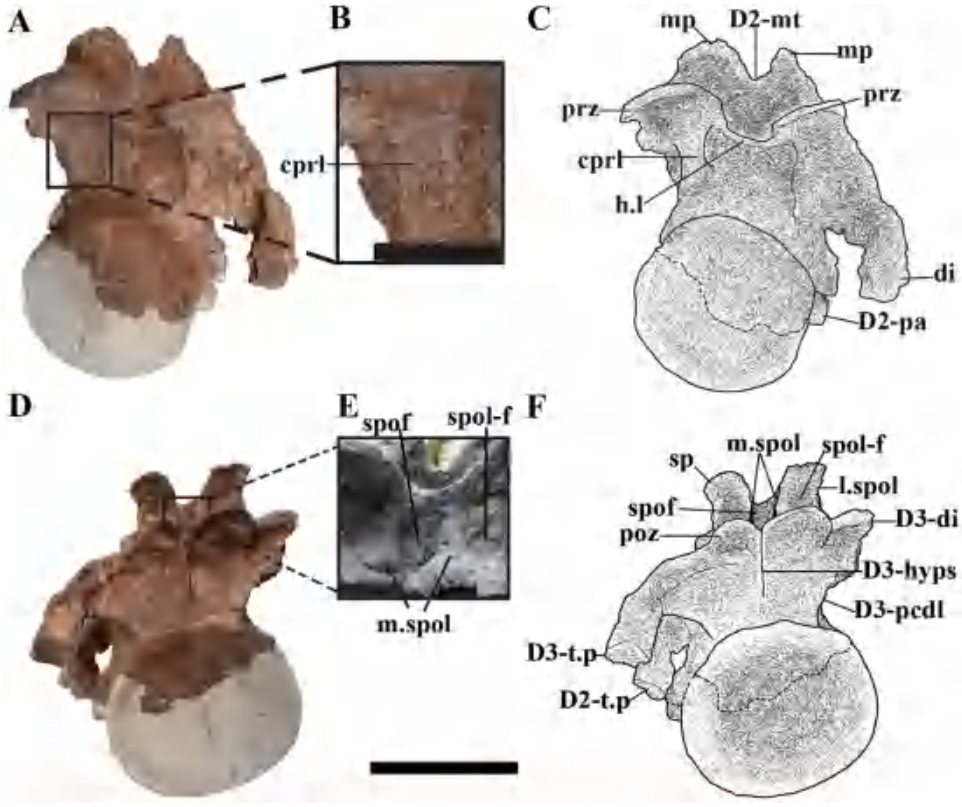

Figure 5. Dorsal vertebrae 2–3 of *Xinjiangtitan shanshanesis* (SSV12001) in anterior and posterior views. A, anterior view of dorsal 2; B, close-up of the centroprezygapophyseal lamina of dorsal 2; C, schematic of anterior view of dorsal 2; D, posterior view of dorsal 3; E, close-up of middle spinodiapophyseal laminae of dorsal 3; F, schematic of posterior view of dorsal 3. Scale bars: A, C, D, F, 30 cm; B, 10 cm; E, not to scale.

spinopostzygapophyseal lamina (M. SPOL). The M. SPOL differs from that in *Rebbachisaurus garasbae* (MNHN-MRS 1980) (Wilson 2012), which is thinner, longer and more vertical than that of *Xinjiangtitan*. It is also different from the postspinal lamina perpendicular to the midline of the postzygapophyses in *Diplodocus* (Hatcher 1901; Gilmore 1936) and *Euhelopus zdanskyi* (Wilson and Upchurch 2009). The M. SPOLs bound a small deep spinopostzygapophyseal fossa (SPOF) (Figure 5D, 5E, 5F). The M. SPOL and the L. SPOL define a shallower intralaminar fossa inbetween on each side, which should be the spinopostzygapophyseal lamina fossa (SPOL-F) (Figure 5E, 5F; Wilson et al. 2011: Fig.9).

The neural spines of dorsals 2–3 bifurcate to a 'trifid' appearance as that on dorsal 1, but the sulcus between the median tubercle and the metapophyses is unconspicuous along with the waning median tubercle and the metapophyses (Figure 6A, 6B). Differ from dorsals 1–2, the TLP of dorsal 3 becomes thin mediolaterally and is not fused to the L. SPOL. The L. SPOL of dorsal 3 originates from the lateral margin of the TLP to the dorsolateral part of postzygapophyses. In dorsal or posterior views, the TLP of dorsal 3 projects more posteriorly, so that the angle between the paired TLPs of dorsal 3 becomes smaller than that on dorsals 1–2.

Dorsal vertebrae 4-9

The dorsal vertebrae 4–9 can be distinguished from the first three dorsal vertebrae on the basis of several features: the centra of dorsals 4–9 are shorter and have more concave lateral surface than those of dorsals 1–3; the pleurocoels of dorsals 4–9 become smaller but deeper than that of dorsals 1-3, migrating to the most anterodorsal parts of the centra and next to the anterior condyles of the centra; the pleurocoel of dorsal 4 is well defined, while those of dorsals 5–6 are not sharply bounded dorsally; the transverse processes shorten mediolaterally protruding nearly horizontally and elevate to the dorsal portions of the neural arches, while the terminal portions extend posterolaterally to the level with the intervertebral boundary; the parapophysis from dorsal 4 to succeeding dorsals is completely on the neural arch; the neural arches continue to increase their heights dorsoventrally and share more complex fossae and laminae structure (Figures 7, 8); the degree of bifurcation of the neural spines decreases gradually.

Dorsals 4-6

These three dorsal vertebrae are preserved in articulation. The anterior condyle of dorsal 4 is about 37% of the minimus length of centrum, and the posterior cotyle of the centrum of dorsal 6 bears an obvious flange with the lateral surface of centrum (Figure 7). The right lateral and ventral surfaces of centra of dorsals 4-6 are missing.

The neural arches of dorsals 4–6 are more elongated dorsoventrally and narrower transversely than the previous dorsal vertebrae, this trend gradually increases from dorsal 4 to dorsal 6. In the left lateral view, the elongated parapophysis of dorsal 4 positions on the anterodorsal portion of the neural arch with an oval concave facet. Conversely, only the bases of the parapophyses in dorsals 5–6 are preserved, but they position more anterodorsally than that on the previous dorsal vertebrae. The transverse processes present as relatively shorter and thicker processes than those in dorsals 1–3 and are adjacent to the prezygapophyses.

The prezygapophyses of dorsal 4 project not as anteriorly as those in dorsal 2, but the articular facets are poorly preserved with different sizes due to diagenetic deformation. The hypantrum presents as a 'Y'-shaped lamina articulated with the hyposphene in dorsal 3. In anterior view, the prezygapophyses are supported by the

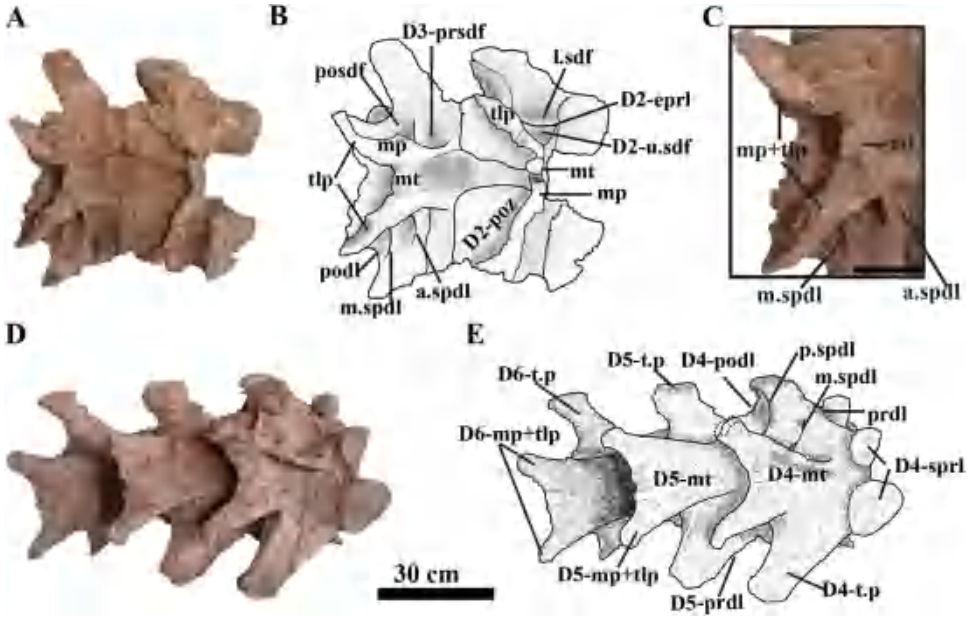

Figure 6. Dorsal vertebrae 2–6 of *Xinjiangtitan shanshanesis* (SSV12001) in dorsal views. A, dorsal view of dorsals 2–3; B, schematic of dorsal view of dorsals 2–3; C, close-up of neural spine of dorsal 3; D, dorsal view of dorsals 4–6; E, schematic of dorsal view of dorsals 4–6. Scale bars: A-B, D-E, 30 cm; C, 10 cm.

PRDL dorsolaterally, the PRPL ventrolaterally and the CPRL ventrally. The PRPL, the CPRL and the parapophysis bound an elongated parapophyseal centroprezygapophyseal fossa (PACPRF) (Figure 7A), which is adjacent to a deep triangular centroprezygapophyseal fossa (CPRF) defined beneath the prezygapophysis (Figure 8A, 8B, 8C). In lateral or dorsal view, the SPRL is well developed as a thickened lamina.

The prezygoparapophyseal lamina (PRPL) and the PRDL are well developed, forming the anteroventral margin, posterodorsal margin of the prezygapophyseal paradiapophyseal fossa (PRPADF), respectively, in dorsal 4, but this fossa is not blind ventrally due to lacking the PPDL (Figure 7A, 7D). In addition to the forementioned laminae, the PODL, the PCDL and the posterior centroparapophyseal lamina (PCPL) are well developed in dorsal 6 in right lateral view (Figure 7D). Furthermore, there are horizontal bipartite PCPLs with a thick dorsal lamina and a thin ventral lamina in dorsal 6: the ventral PCPL forms the ventral margin of the parapophyseal centrodiapophyseal fossa (PACDF) and the dorsal margin of the centroparapophyseal fossa (CPAF); the dorsal PCPL subdivides the PACDF (Figure 7D, 7F). Laterally, the transverse process meets the postzygapophysis via a short PODL. The M. SPDLs present in dorsals 4–5 subdividing the SDF into PRSDF and POSDF as that in dorsal 3, but differently, the M. SPDL of dorsal 4 is dorsally bifurcated (bif.M. SPDL) contracting the SPRL in left lateral view (Figure 7A, 7B, 7C). Furthermore, the transverse process of dorsal 4 also develops the posterior spinodiapophyseal

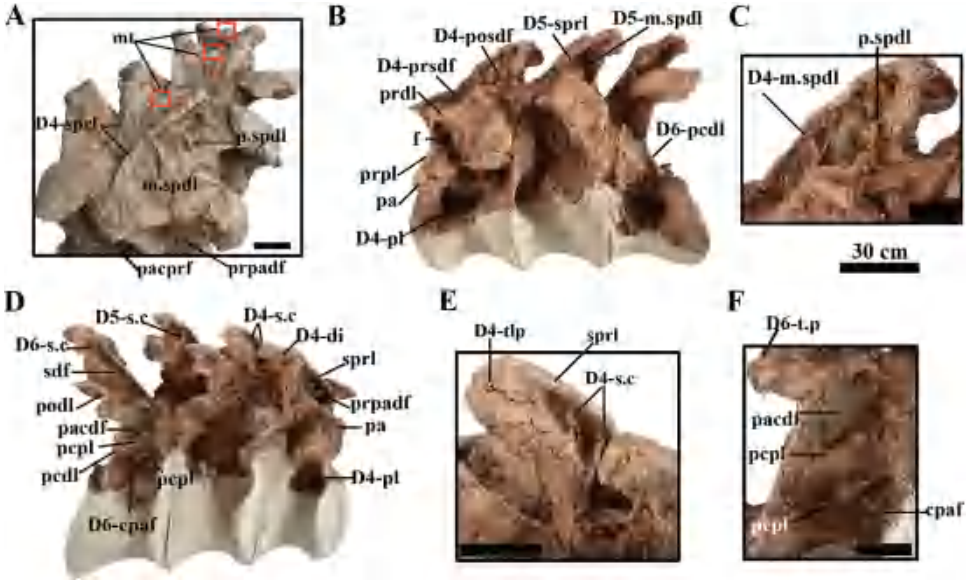

Figure 7. Dorsal vertebrae 4–6 of *Xinjiangtitan shanshanesis* (SSV12001) in lateral views. A, anterodorsal lateral view of dorsals 4–6; B, left lateral view of dorsals 4–6; C, close-up of left spinodiapophyseal fossa of dorsal 4; D, right lateral view of dorsals 4–6; E, close-up of right spinodiapophyseal fossa of dorsal 4; F, close-up of right neural arch of dorsal 6. Scale bars: A, C, E, F, 10 cm; B, D, 30 cm.

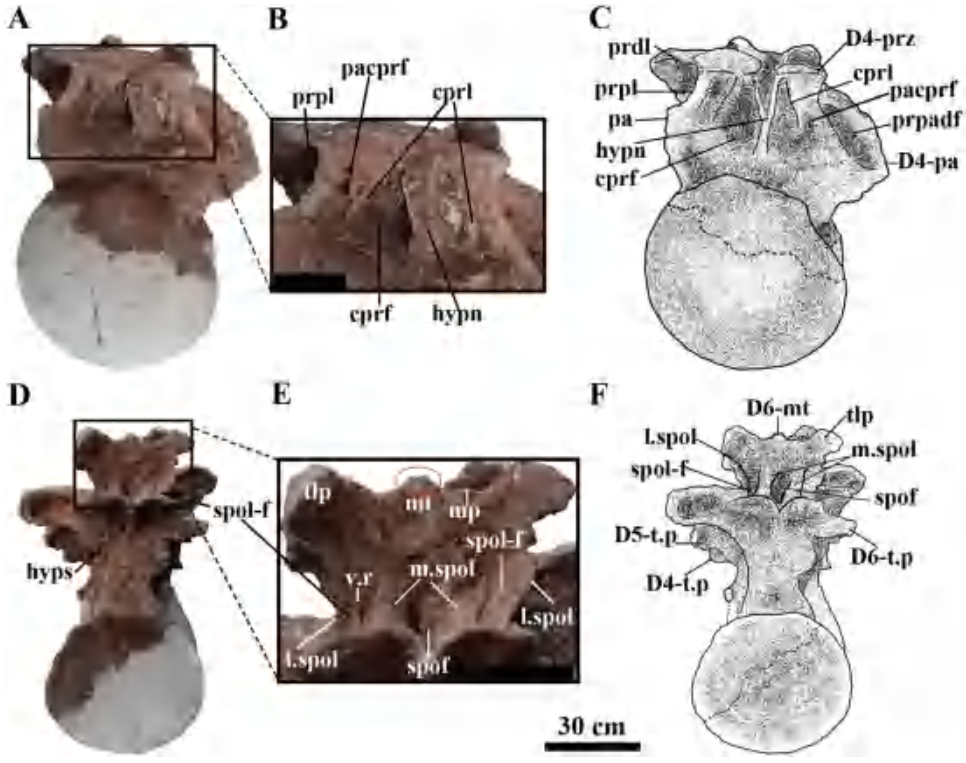

Figure 8. Dorsal vertebrae 4–6 of *Xinjiangtitan shanshanesis* (SSV12001) in anterior and posterior views. A, anterior view of dorsal 4; B, close-up of anterior neural arch of dorsal 4 in anterior view; C, schematic of anterior view of dorsal 4; D, posterior view of dorsal 6; E, close-up of neural spine of dorsal 6 in posterior view; F, schematic of posterior view of dorsal 6. Scale bars: A, C, D, F, 30 cm; B, E, 10 cm.

laminae (P. SPDL) in left lateral view, which originates from the posterior margin of transverse process to meet the upper half of the SPRL (Figure 7C). In the right lateral view of dorsals 4–6, the P. SPDL is replaced by some sloping secondary crests (S.C) at the dorsal end of the SDF; this condition is similar to that in dorsal 3 (Figure 7D, 7E).

In posterior view, the paired postzygapophyses of dorsal 6 connect to each other as that in dorsal 3, but the vertical hyposphene is badly preserved, and the CPOL is not preserved. The articular surface of the postzygapophysis is slightly concave and oriented ventrally. The L. SPOL and the M. SPOL are well developed as that in dorsal 3. The sturdier M. SPOL mainly develops on the dorsal portion of the postzygapophyses, so that the enclosed SPOF is relatively small. In addition, a vertical secondary ridge (V.R) can be discerned in the SPOL-F adjacent to the M. SPOL (Figure 8D, 8E, 8F).

Differs from the preceding dorsal vertebrae, the bifurcation with wider and shallower median concave between the median tubercle and the metapophyses of the three dorsal vertebrae weakens gradually as a 'U'-shaped cleft in dorsal view (Figure 6D, 6E). Whereas in the posterior view, the median tubercle of dorsal 6 becomes a smaller tip and the bifurcation of the neural spine appears obvious 'W'-shaped (Figure 7A). The metapophyses are simply developed merged with the TLPs, but the TLPs present as shorter paddle-shaped processes extending prominently posteriorly, rather than the triangular lateral process present in previous dorsals (Figure 8D, 8E, 8F).

Dorsals 7-9

Dorsals 7–9 are preserved in articulation, but the right lateral lower portions of the centra of dorsals 7–8 are reconstructed by plaster. The centra of these three dorsal vertebrae are shorter anteroposteriorly than the aforementioned dorsal vertebrae. However, the length of the centrum of dorsal 9 shortens abnormally due to distortion (Figure 9). Laterally, the smaller and deeper pleurocoels ascend to the higher level relative to that on the previous dorsal vertebrae (Figures 10 B; 10A). The ventral surfaces of dorsals 8–9 are smooth and concave without the ventral keel (Figure 11E).

The height of the neural arch increases obviously from dorsal 1 to dorsal 9, measured from the dorsal margin of the centrum to the base of the postzygapophyses. A deep PACDF is developed posteriorly to the parapophyses and ventrally to the PRDL in dorsals 7-9 (Figure 9B, 9D). The PRPL of dorsal 7 presents as a stout lamina, the short PPDL contacts the posterior margin of the prezygapophysis and the anterior margin of the transverse process. The parapophysis with a suboval-shaped articular facet situates at the most anterior portion of the arch just posteroventrally to the prezygapophysis. The PRPADF becomes very shallow with the elevation of the parapophysis (Figure 9A). Laterally, the anterior centroparapophyseal lamina (ACPL) forms the anterior border of the neural arch in dorsal 7 (Figure 9B), and interestingly, there are bipartite PCPLs on the right side of the neural arch of dorsal 7 with a thin dorsal lamina subparallel to a robust ventral lamina (Figure 10A). The single thick PCPL of dorsal 8 is represented by its posteroventral portion that joins the almost vertically directed PCDL (Figure 9B, 9D). In dorsal 9, the ACPL and the PCPL are well developed as single laminae, forming the triangular centroparapophyseal fossa (CPAF) posteroventral to the parapophysis (Figure 9B, 9D). The transverse processes of dorsals 7–9 position in the level of the postzygapophyses, projecting horizontally as short robust processes with rough articular surfaces. In contrast to the previous dorsal vertebrae, the A. SPDL, the P. SPDL and the M. SPDL are absent in dorsals 7–9, and the SDFs appear as single large and deep fossae. Only a sloping secondary crest develops in the dorsal end of the right SDF of dorsal 7 (Figure 10A). In the left lateral view of dorsal 8, a robust SPRL

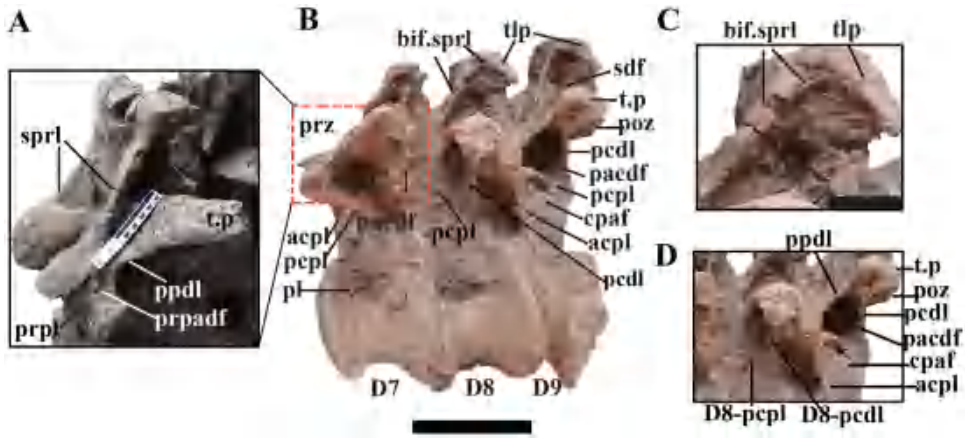

Figure 9. Dorsal vertebrae 7–9 of *Xinjiangtitan shanshanesis* (SSV12001) in left lateral view. A, close-up of left dorsolateral view of the parapophyseal centrodiapophyseal fossa of dorsal 7; B, left lateral view of dorsals 7–9; C, close-up of left spinoprezygapophyseal lamina of dorsal 8; D, close-up of left lateral view of laminae of dorsals 8–9. Scale bars: A, C, 10 cm; B, 30 cm; D, not to scale.

bifurcates dorsally into two branches, an anterior sturdy branch connecting the metapophyses of the neural spine and the posterior thin branch connecting the dorsolateral portion of the TLP of the neural spine (Figure 9B, 9C). Despite serial variability in the development of the bifurcated SPRL (bif.SPRL), we consider this may be an autapomorphy of *Xinjiangtitan*.

The left prezygapophysis of dorsal 7 is not the same size as the right prezygapophysis due to distortion. The articular surfaces of the prezygapophyses are slightly convex. Unlike the previous dorsal vertebrae, the hypantrum of dorsal 7 appears as a single vertical lamina that widens transversely in its upper part and tapers in the lower part (Figure 10B,

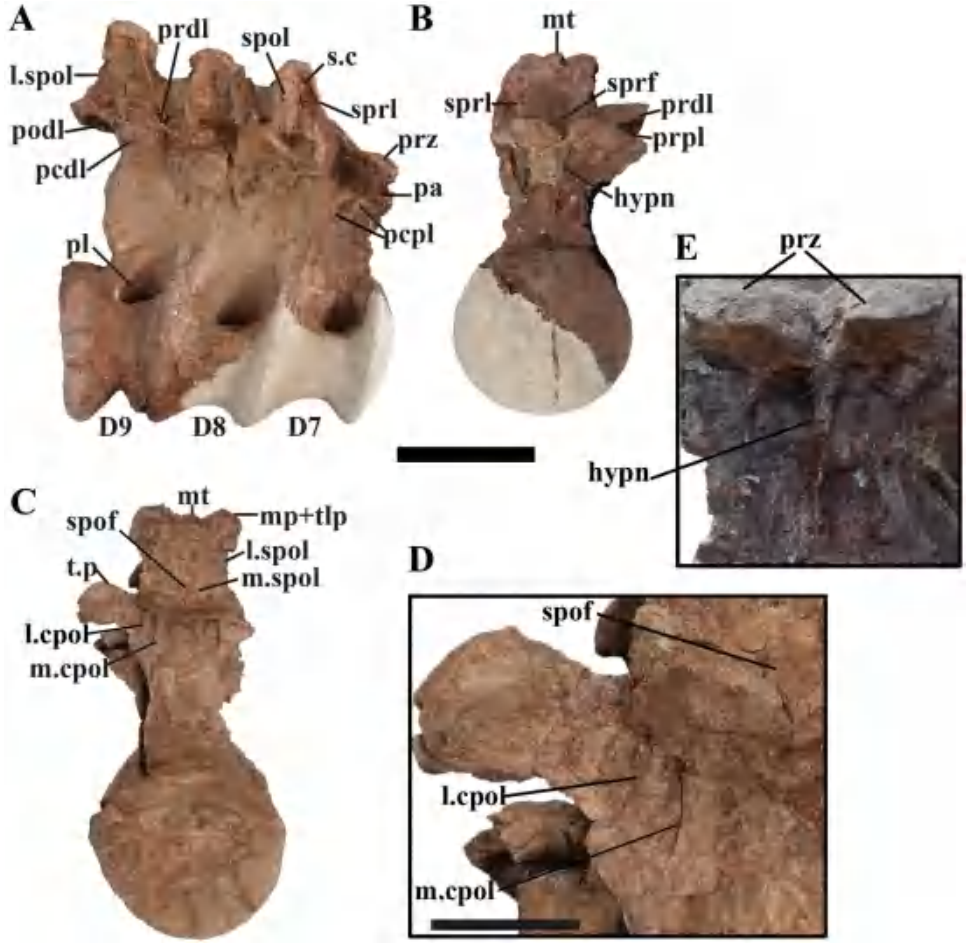

Figure 10. Dorsal vertebrae 7–9 of *Xinjiangtitan shanshanesis* (SSV12001) in right, anterior and posterior views. A, right lateral view of dorsals 7–9; B, anterior view of dorsal 7; C, posterior view of dorsal 9; D, close-up of posterior view of the centropostzygapophyseal laminae of dorsal 9; E, close-up of anterior view of the hypantrum of dorsal 7. Scale bars: A-C, 30 cm; D, 10 cm; E, not to scale.

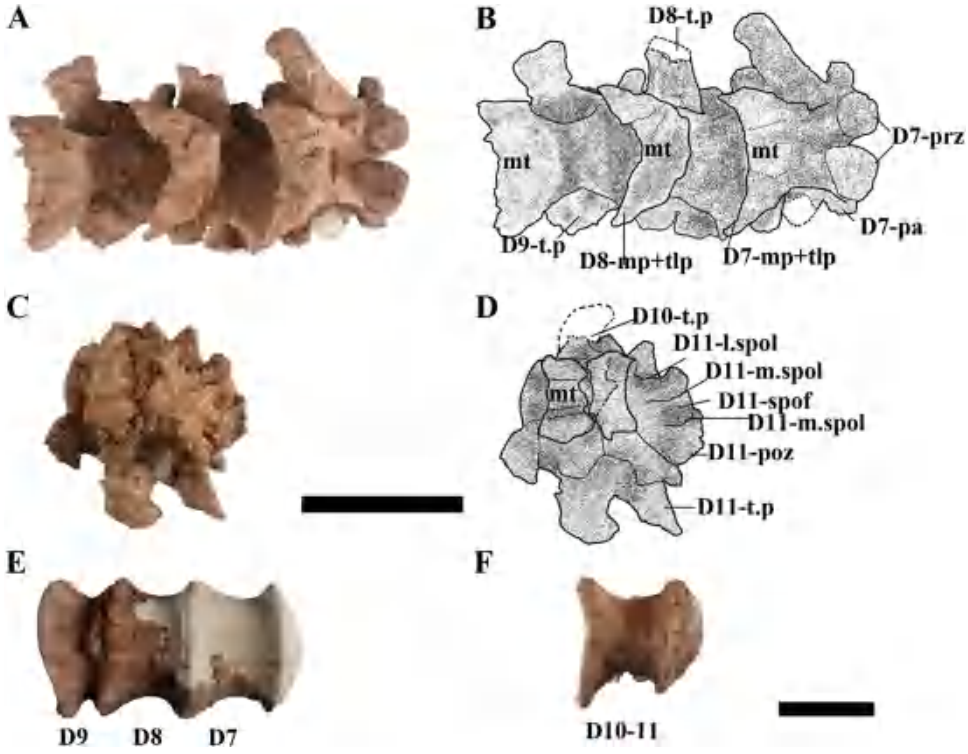

Figure 11. Dorsal vertebrae 7–11 of *Xinjiangtitan shanshanesis* (SSV12001) in dorsal and ventral views. A, dorsal view of dorsals 7–9; B, schematic of dorsal view of dorsals 7–9; C, dorsal view of dorsals 10–11; D, schematic of dorsal view of dorsals 10–11; E, ventral view of dorsals 7–9; F, ventral view of dorsals 10–11. Scale bar: A-F, 30 cm.

10E), while the hypothesis is not preserved in dorsal 9 in posterior view (Figure 10C, 10D). The SPRLs extend posteriorly and dorsally and terminate at the base of the anterior margin of neural spine to form a dorsoventrally elongated spinoprezygapophyseal fossa (SPRF). In posterior view, the postzgapophyses of dorsal 9 connect to each other as in dorsals 4–6. The left postzygapophysis is supported ventrally by the two stout CPOLs: one is a medial centropostzygapophyseal lamina (M. CPOL) just under the postzygapophysis, and the other one is a lateral centropostzygapophyseal lamina (L. CPOL) extending from the ventrolateral margin of the postzygapophysis down to the PCDL, while only the L. CPOL is preserved under the right postzygapophysis. The L. SPOL, the M. SPOL and the SPOF are developed as that on previous dorsal vertebrae (Figure 10C, 10D).

The heights of the neural spines increase sequentialy in these three dorsal vertebrae, but the bifurcation of neural spines weakens obviously. The median tubercle appears as sub-tetragonal processes, and the sulcus between the median tubercle and the metapophyses is narrow and shallow. The metapophyses are poorly developed, but the TLPs extend posteroventrally along the lateral margin of the neural spines as acute triangular processes (Figure 9B, 9C). The whole median portion of the spine elongates anteroposteriorly. In dorsal view, the bifurcations of the neural spines of dorsals 7–9 are weaker than those on previous dorsals and are crescentic shaped, neither the 'W'-shaped in dorsals 1–3 nor the 'U'-shaped in dorsals 4–6. Whereas in posterior view, they are stronger 'W'-shaped cleft than those in dorsals 2–4, and almost similarly developed as dorsals 5–6.

Dorsal vertebrae 10-12

These three dorsal centra shorten anteroposteriorly with markedly concave lateral and ventral surfaces. The small and deep pleurocoels locate on the most-anterodorsal lateral parts of the centra, but they are not sharply defined dorsoposteriorlly. The neural arch pillars are lower than the middle dorsal vertebrae. The nearly parallel CPOLs are absent, may be due to preservation and preparation. The neural spines of dorsal 10 to dorsal 12 are unbifurcated with the height bigger than the previous dorsals.

Dorsals 10-11

The two dorsal vertebrae are articulated preserved by anteroposteriorly diagenetic compression with evidently anteroposteriorly shortened centra, so they were considered as one vertebra in the original description (Wu et al. 2013). However, it is observed that the two vertebrae are not fused into one with a clear boundary between the two centra.

The anterior condyle of dorsal 10 is prominently convex, about 70% of the minimus length of centra (exclude the anterior condyle), with a developed flange boundary to the lateral surface. In anterior view, the centrum exhibits camellate internal architecture, which is infilled with matrix as *Mamenchisaurus hochuanensis, Mamenchisaurus youngi* (Young and Chao 1972; Ouyang and Ye 2002). The anterior condyle is taller than wide, but the deeply concaved posterior articular surface of dorsal 11 is wider than height with prominent flange (Figure 12A, 12B). The pleurocoels of dorsals 10–11 invade the most anterior portion of the centra, the anterior margin of which is bounded by the posterior margin of the anterior condyle. Moreover, the pleurocoels are much deeper and almost penetrate the centrum than the aforementioned dorsals (Figure 12A, 12B, 12C, 12D). Ventrally, the centra of dorsals 10–11 are smooth without ventral keel (Figure 11F).

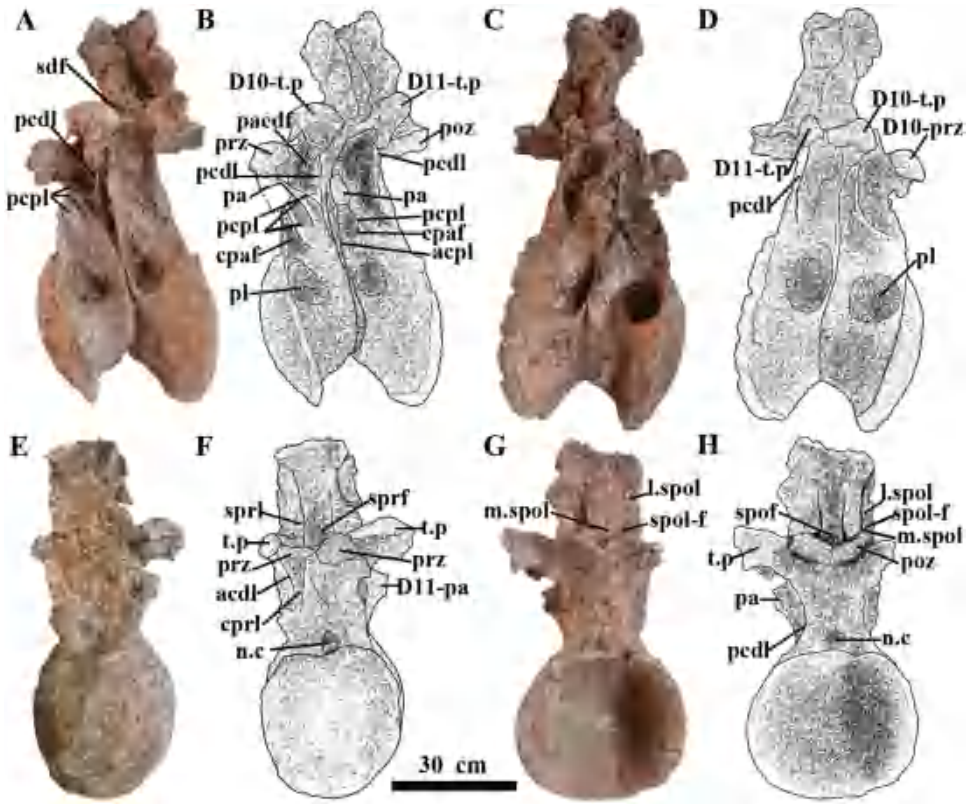

Figure 12. Dorsal vertebrae 10–11 of *Xinjiangtitan shanshanesis* (SSV12001). A, left lateral view of dorsals 10–11; B, schematic of left lateral view of dorsals 10–11; C, right lateral view of dorsals 10–11; D, schematic of right lateral view of dorsals 10–11; E, anterior view of dorsal 10; F, schematic of anterior view of dorsal 10; G, posterior view of dorsal 11; H, schematic of posterior view of dorsal 11. Scale bar: A-H, 30 cm.

The heights of the neural arches increase compared with the aforementioned dorsals and the laminae are developed. In anterior view, the incomplete hypantrum is faintly developed below the prezygapophyses. Only the right CPRL is preserved as a vertical ridge. The oval neural canal is elongated dorsoventrally (Figure 12E, 12F). In lateral view, the ventral portion of parapophysis of dorsal 10 is damaged. The right side of dorsal 11 shares a single PCPL, while that of dorsal 10 exhibits triplicated PCPLs, with a thin dorsal lamina subparallel to the other two laminae. The dorsal PCPL extends posteroventrally to contact the PCDL producing the ventral boundary of the PACDF, the middle one extends posteroventrally to bound the posterior margin of the CPAF, and the robust ventral lamina subdivides the CPAF (Figure 12A, 12B). This condition is more complex than the bipartite PCDLs in dorsal 7, somewhat similar to the case of dorsals 9–11 in *Klamelisaurus gobiensis* (Moore et al., 2020: Fig. 11). The parapophysis of dorsal 11 is well developed as a short rod-like-shaped process with an elongated dorsoventrally concave articular surface, which is supported by ACPL anteroventrally and PCPL posteroventrally. The ACPL, the PCPL and the parapophysis enclose a shallow CPAF on the anterolateral surface of the centrum (Figure 12A, 12B). The transverse processes of dorsals 10–11 are short robust processes projecting laterally, the transverse processes of dorsal 11 are shorter mediolaterally than that of dorsal 10. The articular surface of the transverse process of dorsal 10 faces ventrolaterally, while that of dorsal 11 is projected laterally.

The prezygapophyses of dorsals 10–11 are not well preserved, and the articular surfaces are difficult to identify, but the partial SPRL is preserved to define a small SPRF. The postzygapophyses of dorsal 11 connect to each other as the condition in the aforementioned dorsal vertebrae. However, the hyposphene, the L. CPOL and the CPOL are not preserved, may be due to respiration. The neural spines of dorsals 10–11 are no longer bifurcated and are rectangle-shaped in dorsal view (Figure 11C, 11D). The SDF can be recognised at the base of the spine in dorsal 10. In posterior view, the L. SPOL, the M. SPOL and the SPOL-F are developed as that on the aforementioned dorsal vertebrae. The SPOF is developed even though it shortens dorsoventrally (Figure 12G, 12H).

Dorsal 12

The dorsal 12 is poorly preserved, represented by the centrum, prezygapophyses, left parapophysis and partial neural arch. It is the last dorsal vertebra, marking the dorsosacral transition. The anterior condyle of centrum is prominently convex, about half of the minimum length of the centrum. The outline of anterior condyle and posterior articular surface are subcircular. The posterior facet bears a more obvious flange with the lateral surface of centrum than that of the anterior condyle. In lateral view, the lateral surface of the centrum is prominently concave. The depth of the pleurocoel rapidly increases across dorsals 10–12. The ventral surface of the centrum is distinctly concave (Figure 13C).

The remnant of the neural arch is more compressed anteroposteriorly than the previous dorsal vertebrae. The prezygapophyses project anterodorsally, with the subcircular and slight convex articular surface (Figure 13A). In the left lateral view, the parapophysis is damaged distally and positions at the lower portion of the neural arch. The PRPL extends from the lateral edge of the prezygapophysis to the anterodorsal portion of the parapophysis (Figure 13A, 13B).

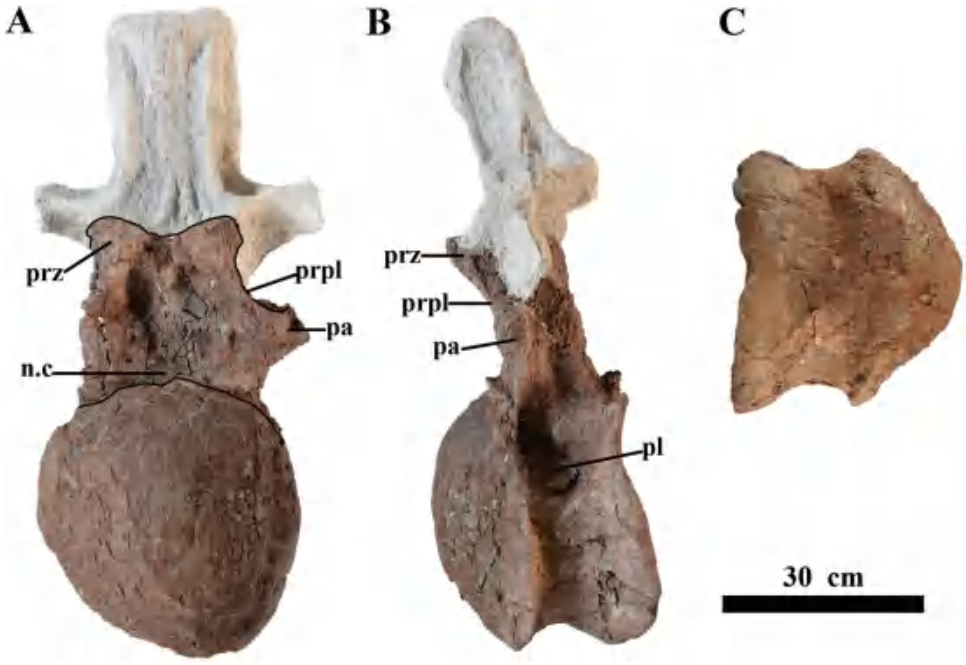

Figure 13. Dorsal vertebrae 12 of *Xinjiangtitan shanshanesis* (SSV12001). A, anterior view of dorsal 12; B, left lateral view of dorsal 12; C, ventral view of dorsal 12. Scale bar: A-C, 30 cm.

Dorsal ribs

Five isolated, partial dorsal ribs were found disarticulated, but none of them is directly associated with any particular dorsal vertebra. There are four left ribs preserved belong to the anterior part of the series, and one is the right rib of the anterior dorsal series according to its curvature and shaft diameter. The right one is represented by the proximal plate and an elongated portion from the top of the shaft, whereas the other four dorsal ribs only represented by the base of the proximal plate. The following description is mainly based on the right one because it is better preserved. The proximal portion of the shaft of rib presents as 'Y'-shaped with maximum width of the proximal shaft (47 cm) (measured from the proximal end of the tubercle and capticulum). The anterior surface of the shaft is convex and the posterior surface is concave (Figures 14A, 14B). The capitulum and tuberculum are relatively strong, forming an acute angle depression between them at the rib head; this depression is similar to that in *Klamelisaurus gobiensis* (Moore et al. 2018) and *Bellusaurus sui* (Moore et al. 2020: Fig. 14), but lacks the subparallel ridge within the depression due to breakage.

The tuberculum is shorter than the capitulum with transversely oval articular facet. Both tuberculum and capitulum possess prominent ridges. In anterior view, the tuberculum forms a sharp ridge continued after the depression along the shaft. The distance between the highest point of this ridge and the proximal end of the tuberculum is 24 cm. The other robust ridge starts from the end of depression in the direction to the capitulum. In lateral view, a proximodistal ridge extends from the tuberculum to the distal of the shaft, forming the lateral boundary of the shaft (Figure 14D). The rib shaft is widened anteroposteriorly and compressed mediolaterally, similar to the anterior dorsal rib in titansauriform sauropods, such as *Dinheirosaurus lourinhanensis* (Manion et al. 2012). There is a small and deep pneumatic fossa (PF) placed at the base of the acute ridge (Figure 14A, 14C, 14E,). The rib shaft is broken, and the cross-sectional shaft is subtriangular with very limited pneumaticity (Figure 14F).

Phylogenetic analysis

In order to assess the phylogenetic relationships of *Xinjiangtitan* and other mamenchisaurid sauropods, we scored them for modified versions of datasets of *Hudiesaurus* (Upchurch et al., 2021). Dataset 1 of Upchurch et al. 2021 (update from Mannion et al. 2019) is based on Mannion et al. (2019) which originally comprises 124 taxa scored for 548 characters. Upchurch et al. (2021) added three taxa: *Hudiesaurus, Rhomaleopakhus* and *Xinjiangtitan*, scored for 551characters. Dataset 2 of Upchurch et al. 2021 (update from GEA of Moore et al. 2020) is the updated matrix of GEA of Moore et al. (2020) consisting of 106 taxa scored for 444 characters. The revised data matrices are provided as TNT files (Supplementary Data 1 and 2 for dataset 1 of Upchurch et al. 2021(updated; Mannion et al. 2019) and dataset 2 of Upchurch et al. 2021 (updated Moore et al. 2020) respectively), with stored settings for assigning characters as ordered or inactive.

Phylogenetic analyses were carried out in TNT V.1.5 (Goloboff et al. 2008; Goloboff and Catalano 2016). The New Technology Search was applied first, setting 50,000 maximum trees. Searches employed sectorial searches, drift, and tree fusing, with the consensus stabilised 10 times. Both matrices were analysed in a maximum parsimony framework. This yielded 32 trees of length 2729 steps in the dataset 1 of Upchurch et al. 2021 (update from Mannion et al. 2019 matrix), 23 trees of length 2120 steps in the dataset 2 of Upchurch et al. 2021 (update from GEA of Moore et al. 2020). In order to research for additional topologies, the resulting 32 MPTs and 23 MPTs were, respectively, then used as the starting trees for a traditional search using TBR on the trees in RAM. Finally, analysis of the dataset 1 of Upchurch et al. 2021 (update from Mannion et al. 2019) produces 50,000 most parsimonious trees (MPTs) with lengths of 2729 steps and analysis of the dataset 2 of Upchurch et al. 2021 (update from GEA of Moore et al. 2020) produces 50, 000 most parsimonious trees (MPTs) with lengths of 2120 steps. Strict consensus tree was obtained by consensus analysis of all parsimony trees. Character mapping was carried out in Mesquite version 2.75.

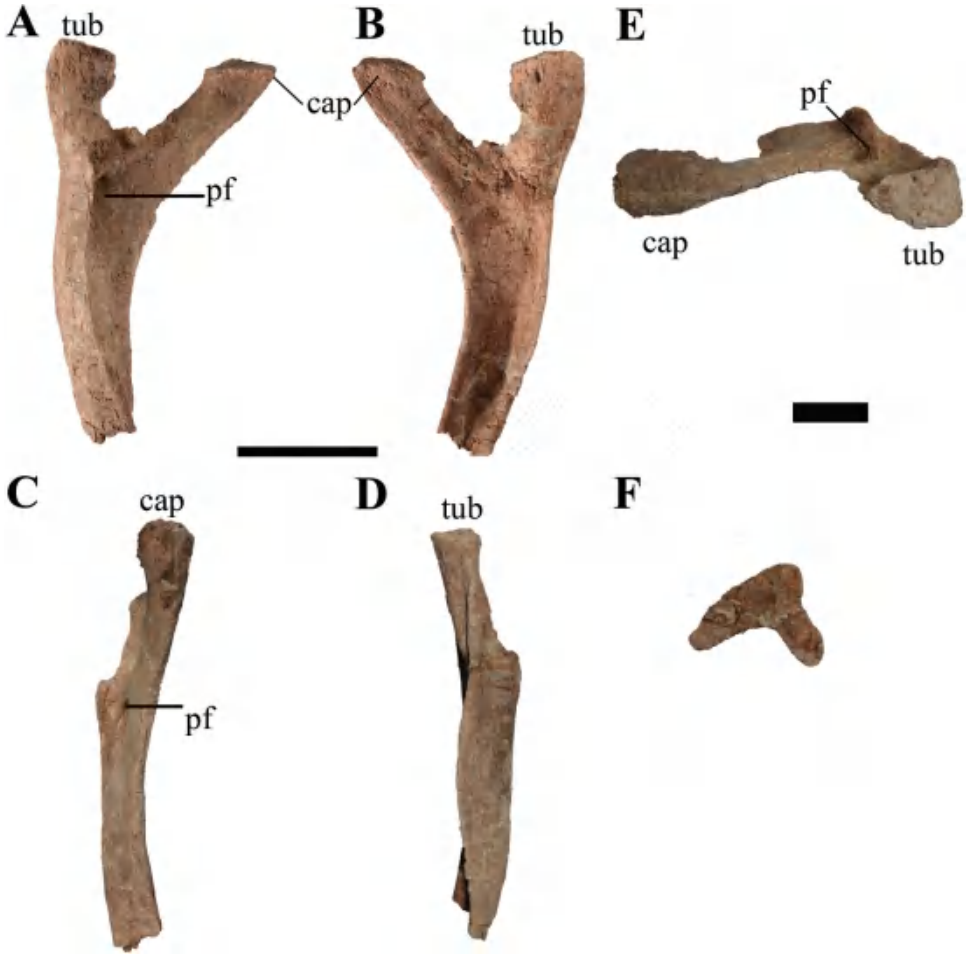

Figure 14. Right dorsal rib of *Xinjiangtitan shanshanesis* (SSV12001). A, anterior view; B, posterior view; C, medial view; D, lateral view; E, proximal view; F, distal view. Scale bars: A-D, 30 cm; E-F, 10 cm.

We revised four scorings of cervical vertebrae of *Xinjiangtitan* in the dataset 1 of Upchurch et al. 2021 (update from; Mannion et al. 2019) (1/2 to 2 (Ch.122), 1 to 0/1 (Ch.128), 0/1 to 1 (Ch.129), ? to 0 (Ch.137)), 60 scorings of dorsal vertebrae of *Xinjiangtitan* in the dataset 1 of Upchurch et al. 2021 (update from; Mannion et al. 2019) (? to 1 (Ch.22, Ch.23, Ch.145, Ch.155, Ch.159, Ch.161, Ch.162, Ch.163, Ch.165, Ch.166, Ch.168, Ch.169, Ch.170, Ch.336, Ch.338, Ch.339, Ch.345, Ch.466, Ch.469, Ch.476, Ch.482, Ch.485, Ch.486); ? to 0 (Ch.142, Ch.144, Ch.146, Ch.149, Ch.150, Ch.151, Ch.152, Ch.156, Ch.157, Ch.158, Ch.160, Ch.164, Ch.332, Ch.333, Ch.334, Ch.337, Ch.340, Ch.341, Ch.342, Ch.344, Ch.467, Ch.468, Ch.470, Ch.471, Ch.472, Ch. 473, Ch.475, Ch.477, Ch.478, Ch.479, Ch.480, Ch.481, Ch.483, Ch.484);? to 2 (Ch.147), ? to 1&2 (Ch.148), ? to 0&1 (Ch.474), and one scoring of dorsal rib of *Xinjiangtitan* in the dataset 1 of Upchurch et al. 2021 (update from; Mannion et al. 2019) (? to 0 (Ch.487). We scored sixty-five characters of dorsal vertebrae and one characteristic of dorsal rib of *Xinjiangtitan* in this matrix.

The mamenchisaurid clade is supported by nine synapomorphies ('0' to '1' for character 128,155,199,212,214,233,465; '0' to '2' for character 27; '0/1' to '2' for character 147), two of which are cervical characters (Cervical neural arches (post-Cv3), epipophyses extend beyond the posterior margin of the postzygapophyses (usually as prongs) (character 128); one of which is about cervical rib (Anterior–middle cervical ribs, tuberculum is oriented posterodorsally in lateral view (character 465)), and two characters belong to dorsal vertebrae (Middle-posterior dorsal centra, anterior articular face shape is strongly convex, with degree of convexity approximately consistent along the dorsal sequence (character 147); Middle-posterior dorsal diapophyses are directed laterally or slightly upwards (character 155)).

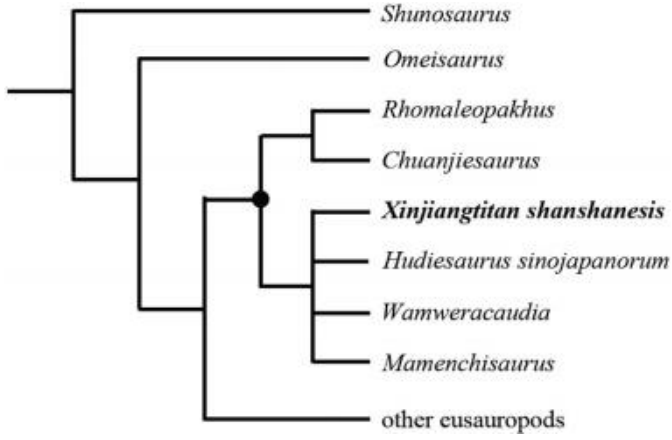

Figure 15. Strict consensus tree for *Xinjiangtitan shanshanensis* produced after dataset 1 of Upchurch et al. 2021 (update from Mannion et al. 2019).

Xinjiangtitan is recovered in a polytomy with *Hudiesaurus*, *Mamenchisaurus*, and *Wamweracaudia*, with this the sister clade to (*Chuanjiesaurus* + *Rhomaleopakhus*) (Figure 15). The *Chuanjiesaurus* and *Rhomaleopakhus* clade within

Mamenchisauridae is supported by two synapomorphies of cervical and dorsal vertebrae ('0' to '1' for character 44, 51): 'Radius to humerus proximodistal length ratio is less than 0.65 (character 44)'; 'Ulna, ratio of mediolateral width of proximal end (equivalent to anteromedial arm) to anteroposterior width of proximal end (equivalent to anterolateral arm) is 1.4 to <2.0 (character 51)'. The *Xinjiangtitan, Hudiesaurus, Mamenchisaurus* and *Wamweracaudia* clade is supported by seven synapomorphies ('0' to '1' for character 26,140,159,323,355; '1' to '0' for character 391; '2' to '3' for character 27): 'Anteriormost caudal centra, lowest average Elongation Index [aEI; centrum anteroposterior length (excluding articular ball) divided by the mean average value of the anterior surface mediolateral width and dorsoventral height] value is 0.6 or greater (character 26)'; 'Anterior caudal centra, anteroposterior length of posterior condylar ball to mean average radius [(mediolateral width + dorsoventral height) divided by 4] of anterior articular surface of centrum ratio is greater than 0.6 (posterior articular surface of centrum is very strongly convex) (character 27)'; 'Cervical ribs, longest shafts extend beneath 3 vertebrae or more (character 140)'); 'Dorsal neural spines, anteroposterior width narrows dorsally to form a triangular shape in lateral view, with the base approximately twice the width as the dorsal tip (character 159)'; cervical 'Postaxial cervical centra, pneumatization of lateral surface is reduced and restricted to less than the anterior two-thirds of the centrum (character 323)'; 'Anteriormost caudal ribs, tubercle on dorsal surface at approximately midlength is present (character 355)'; 'Tibia to femur length ratio is less than 0.6 (character 391)'.

We revised four scorings of cervical vertebrae of *Xinjiangtitan* in the dataset 2 of Upchurch et al. 2021 (update from GEA of Moore et al. 2020) (1/2 to 2 (Ch.122), ? to 0 (Ch.137),? to 1 (Ch.435), ? to 1 (Ch.436)), 40 scorings of dorsal vertebrae of *Xinjiangtitan* in the dataset 2 of Upchurch et al. 2021 (update from GEA of Moore et al. 2020) (0 to 1(Ch.23); ? to 0 (Ch.142, Ch.144, Ch.149, Ch.150, Ch.151, Ch.152, Ch.156, Ch.157, Ch.158, Ch.160, Ch.164, Ch.332, Ch.333, Ch.334, Ch.337, Ch.340, Ch.341, Ch.342, Ch.344, Ch.391, Ch.392); ? to 1 (Ch.145, Ch.155, Ch.159, Ch.161, Ch.162, Ch.163, Ch.165, Ch.166, Ch.168, Ch.169, Ch.336, Ch.338, Ch.339, Ch.345, Ch.390, Ch.393); ? to 2 (Ch.147); ? to 1/2 (Ch.148) and one scoring of dorsal rib of *Xinjiangtitan* in the dataset 2 of Upchurch et al. 2021 (update from GEA of Moore et al. 2020) (? to 1 (Ch.170). Coding of these new characters are based on extensive review of the literatures (e.g. McIntosh 1990; Russell and Zheng 1993; Upchurch 1995; Salgado et al. 1997; Upchurch 1998; Yates 2007; D'Emic 2012; Mannion et al. 2013), as well as our personal observations. See supplemental material for the complete character list and MESQUITE version of the data matrix. Forty-six characters of dorsal vertebrae and one characteristic of dorsal rib of *Xinjiangtitan* were scored in the dataset 2 of Upchurch et al. 2021 (update from GEA of Moore et al. 2020) (Figure 16).

The mamenchisaurid clade is supported by two synapomorphies ('0' to '1' for character 132 and 434), including postaxial cervical and anterior dorsal neural spines that are unbifurcated or bifurcated (character 132); the prezygodiapophyseal lamina (PRDL) of middle and posterior cervical vertebrae in lateral view is convex or with distinct bulging interruption (character 434). The (*Xinjiangtitan* +*Rhomaleopakhus*+ *Hudiesaurus* + *Chuanjiesaurus* + *Wamweracaudia* + *Mamenchisaurus* + *Klameilisaurus* + *Qijianglong* + Shishigou cervicodorsals + Phu Kradung taxon) clade is supported by two synapomorphies ('0' to '2' for character 27,177): 'Anterior caudal centra, anteroposterior

Figure 16. Strict consensus tree for *Xinjiangtitan shanshanensis* produced after dataset 2 of Upchurch et al. 2021 (update from GEA of Moore et al. 2020).

length of posterior condylar ball to mean average radius ([mediolateral width + dorsoventral height] divided by 4) of anterior articular surface of centrum ratio is greater than 0.3 (posterior articular surface of centrum is strongly convex) (character 27)'; 'Anterior caudal centra, posterior articular surface is convex throughout all anterior caudal vertebrae with ribs (character 177)'. This clade is the sister taxon to *Omeisaurus junghiensis* clade within Mamenchisauridae and is supported by one synapomorphy ('0' to '1' for character 323): 'Pneumatization of lateral surface of postaxial cervical centra is reduced and restricted to less than the anterior two-thirds of the centrum (character 323)'.

All of our analyses recover *Xinjiangtitan* as a mamenchisaurid sauropod. Note only characters of the cervical and the dorsal vertebrae of *Xinjiangtitan* were included.

Comparison and Discussion

Comparison

Jurassic sauropods remains are relatively abundant in China, and mamenchisaurids and relevant sauropods are mainly discovered from Shishugou Formation, and Qigu Formation in Xinjiang Uygur Autonomous Region (*Hudiesaurus sinojapanorum* Dong 1997; *Bellusaurus sui* Dong 1990; Mo 2013; Moore et al. 2017; Moore et al. 2018; *Klamelisaurus gobiensis* Zhao 1993; Moore et al. 2020; *Mamenchisaurus sinocanadorum* Russell and Zheng 1993), Lower-Upper Shaximiao Formations and Suining Formation in Sichuan basin (*Mamenchisaurus constructus* Young 1954; Young 1958; Dong 1983; *Mamenchisaurus youngi* Pi et al. 1996; Ouyang and Ye 2002; *Mamenchisaurus hochuanensis* Young and Chao 1972; Dong et al. 1983; *Mamenchisaurus jingyanensis* Zhang et al. 1998; Zhang and Li 2001; *Bashunosaurus* Kuang 2004; *Daanosaurus zhangi* Ye et al. 2005; *Shunosaurus lii* Zhang 1984; *Protognathus oxyodon* Zhang 1988; *Abrosaurus* Ouyang 1989; *Datousaurus bashanensis* Dong and Tang 1984; Cao and You 2000; Peng et al. 2005; *Dashanpusaurus dongi* Peng et al. 2005; *Omeisaurus tianfuensis* He et al. 1988; *Omeisaurus junghsiensis* Young 1939; *Omeisaurus changshouensis* Young 1958; *Omeisaurus maoianus* Tang et al. 2001; *Omeisaurus jiaoi* Jiang et al. 2011; *Omeisaurus puxiani* Tan et al. 2020; *Mamenchisaurus anyuensis* He et al. 1996; *Qijianglong guokr* Xing et al. 2015a; *Yuzhoulong qurenensis* Dai et al. 2022), Hongqin Formation in Anhui province (*Huangshanlong anhuiensis* Huang et al. 2014; *Anhuilong diboensis* Ren et al. 2018), Yan'an Formation in Ningxia Hui Autonomous Region (*Lingwulong shenqi* Xu et al. 2018) and Chuanjie Formation and Zhanghe Formation in Yunnan Province (*Chuanjiesaurus anaensis* Fang et al. 2000; Sekiya 2011; *Analong chuanjieensis* Ren et al. 2020; *Yuanmousaurus jiangyiensis* Lü et al. 2006; *Eomamenchisaurus* Lü et al. 2008; *Nebulasaurus taito* Xing et al. 2015b). Therefore, we selected those taxa whose dorsal vertebrae were preserved for comparison with *Xinjiangtitan*.

Among them, three (*Mamenchisaurus constructus, Mamenchisaurus jingyanensis*, and *Datousaurus bashanensis*) are poorly preserved. In *Mamenchisaurus constructus*, only two articulated dorsal centra and an isolated vertebra with deformed centrum are preserved in the dorsal series. There are some similarities between *Mamenchisaurus constructus* and *Xinjiangtitan*, such as opisthocoelous dorsal centra. However, it is difficult to make a detailed comparison due to the fragmentation and the brief description of *Mamenchisaurus constructus*. The holotype of *Mamenchisaurus jingyanensis* (CV00734) has no dorsal vertebrae preserved, while its paratype (JV002) (Zhang et al. 1998) has several extremely weathered dorsal vertebrae. Differ from well-developed pleurocoels of *Xinjiangtitan shanshanesis*, the pleurocoels are not well developed in dorsal vertebrae, and only anterior neural spines are bifid in *Mamenchisaurus jingyanensis* (Zhang et al. 1998). *Datousaurus bashanensis* (Dong and Tang 1984; Peng et al. 2005; Cao and You 2000

) differs from *Xinjiangtitan* in that the posterior dorsal centra are platycelous with less developed pleurocoels (Dong and Tang 1984: Plate I).

Taxa with better preservation were compared in detail below. In addition, we also compared *Xinjiangtitan* with *Euhelopus zdanski* (Wiman 1929; Wilson and Upchurch 2009) due to similarities of cervical vertebrae between them.

Hudiesaurus sinojapanorum

Initially, it was believed that *Hudiesaurus sinojapanorum* (Dong 1997) was discovered from Kalazha Formation of the Upper Jurassic in Shanshan County of the Turpan Basin, Xinjiang, China. Later studies suggested that fossil bearing formation was probably the Qigu Formation of the Late Jurassic in Shanshan County of the Turpan Basin (Wings et al. 2011; Xing et al. 2015a). The holotype of *Hudiesaurus sinojapanorum* is represented by a complete cervicodorsal vertebra (Dong 1997), which was suggested as the first dorsal vertebra by Dong. However, it was reestimated to be the last cervical vertebra by Upchurch et al. (2021). Dong (1997) classified it as a member of Mamenchisauridae. Upchurch et al. (2021) agreed with this classification (used the term 'core *Mamenchisaurus*-like taxa', refer to Moore et al. 2020), and further confirmed that *Hudiesaurus sinojapanorum* is a sister taxon of *Xinjiangtitan shanshanesis. Hudiesaurus sinojapanorum* and *Xinjiangtitan shanshanesis* share exactly some similar morphological characteristics and close geographic provenance. The holotypy and referred specimen (right forelimb) were collected from two quaries in the same horizon (Dong 1997), while the latter is assigned as the holotype (IVPP V11121-1) of *Rhomaleopakhus turpanensis* (Upchurch et al. 2021). Given the difficulties of identifying the precise position of the isolated vertebra of *Hudiesaurus sinojapanorum*, we compare it with both the last cervical and the first two dorsal vertebrae in *Xinjiangtitan shanshanesis*.

Some similarities present in morphology between *Xinjiangtitan shanshanesis* and *Hudiesaurus sinojapanorum*, for example, the centrum is strongly opisthocoelous and subcircular in outline; the pre-epipophyses are absent; the neural spine bifurcates into three parts, including a small median tubercle and paired metapophyses protruding posterolaterally to form a triangular lateral process (Figure 15A). Comparing to the size of the vertebrae, the maximum anterior posterior length of centrum (including anterior condyle) (466 mm) in *Hudiesaurus sinojapanorum* is longer than that of dorsal 2(330 mm), but much shorter than that of cervical 18 (590 mm) in *Xinjiangtitan shanshanesis*; the transverse width of posterior surface of the centrum of *Hudiesaurus sinojapanorum* (398 mm Upchurch et al. 2021) is similar to that of cervical 18 of *Xinjiangtitan shanshanesis* (390 mm), slightly less than that of dorsal 1 (posterior surface 430 mm) and dorsal 2 (anterior surface 400 mm); the height of postzygapophyses above dorsal margin of centrum in *Hudiesaurus sinojapanorum* (295 mm Upchurch et al. 2021) is greater than that of dorsal 2 of *Xinjiangtitan shanshanesis* (210 mm). Fuctional (excluding anterior convexity) Average Elongation Index (FAEI) is 1.0 in *Hudiesaurus sinojapanorum*, while the posterior width of cervical 18 is uncertain, we calculated the ratio by replacing the posterior width with the anterior width, that of cervical 18 is about 1.1 in *Xinjiangtitan shanshanesis*, and those of dorsals 1–2 are ambiguous due to the ventral portion of centra reconstructed with plaster. The height of the neural spine/

height of the vertebrae of *Hudiesaurus* is 0.54, lower than that of cervical 18 (0.59), dorsal 1(0.62) and dorsal 2(0.67) in *Xinjiangtitan*.

The lateral pleurocoel of *Hudiesaurus sinojapanorum* is largely restricted to the anterior two-thirds of the centrum as that of cervical 18 in *Xinjiangtitan shanshanesis*. The shape of lateral fossa in *Hudiesaurus sinojapanorum* is oval, whereas the latter is semicircle. There is a horizontal lamina (H.L) bounding the pleurocoel dorsally and extending to the anterior end of the pleurocoel merged into the centrum-arch junction, finally both in *Hudiesaurus sinojapanorum* and cervicals17-18 of *Xinjiangtitan shanshanesis*, but unlike the single pleurocoel in dorsal vertebrae of *Xinjiangtitan shanshanesis*. As seen in Figure 2 (Upchruch at al. 2021), this ridge of *Hudiesaurus* extends from slightly anterodorsally to posteroventrally, while that of *Xinjiangtitan shanshanesis* is more horizontally (Figure 2; Upchurch et al. 2021: Fig. 2 A, 2B).

The parapophysis in *Hudiesaurus sinojapanorum* is located at the anteroventral corner of the lateral surface of the centrum as that in cervical 18 of *Xinjiangtitan shanshanesis*, however, which is not preserved in dorsal 1 and elevates to the middle-upper portion of the centra in dorsals 2–3 of *Xinjiangtitan shanshanesis* (Figures 2A and 4) (Upchurch et al. 2021: Fig. 2A, 2B). The transverse processes in *Hudiesaurus sinojapanorum* are shorter and project more laterally slightly in contrast to those of cervical 18, dorsal 1 and dorsal 2 in *Xinjiangtitan shanshanesis*, where the transverse processes are longer mediolaterally, broader anteroposteriorly, and the end portion projects posteroventrally. Steeply inclined ACDLs and PCDLs present both in the cervicodorsal vertebra of *Hudiesaurus sinojapanorum* and cervical18, dorsla1 of *Xinjiangtitan shanshanesis*, but differently, the ACDL in *Hudiesaurus sinojapanorum*, bifurcates into two laminae contracting transverse process ventrally and anteriorly, respectively. In the right lateral view, the PODL is nearly vertical as that in dorsal 1 of *Xinjiangtitan shanshanesis*, unlike that of cervical 18 projects posterodorsally (Figure 2B, 2D).

The prezygapophyses are large and broad with transversely convex articular surface projecting forward beyond the anterior end of the condyle in *Hudiesaurus sinojapanorum*, as well as the cervical 18 and dorsal 2 in *Xinjiangtitan shanshanesis*. Furthermore, in *Hudiesaurus sinojapanorum*, the prezygapophyses have a line of 5–6 adjacent small irregularly shaped coels on their dorsal surface, which was regarded as an autapomorphy (Upchurch et al. 2021). The condition is also present in cervical 18 and dorsal 2 of *Xinjiangtitan shanshanesis* (Figure 18C 18D, 18E). The medial edges of the prezygapophyses descend steeply to meet each other on the midline and form a single TPRL extending down to the top of the neural canal, which partially subdivides the centroprezygapophyseal fossa (CPRF) into left and right subfossae in *Hudiesaurus*. By contrast, in *Xinjiangtitan*, the medial edges of the prezygapophyses of cervical 18 extend medioventrally to form a slightly 'V'-shaped lamina that closely resemble the TPRL of cervicodorsal vertebrae in other sauropods (Wilson 2012), while those of dorsal 2 converge medially to produce a horizontal lamina. It is difficult to identify the two laminae above as the TPRLs given unrepaired the neural canal. The stout single CPRLs in cervicodorsal vertebra *Hudiesaurus sinojapanorum* do not bifurcate at their dorsal ends unlike those of cervical 18 in *Xinjiangtitan shanshanesis*, which is dorsally bifurcated into two subparallel CPRLs (Figure 3D). Whereas, the CPRLs of *Hudiesaurus sinojapanorum* are subparallel with PCDL laterally, this resembles the condition in dorsal 1 of *Xinjiangtitan shanshanesis*, whose CPRL is parallel to the PCDL (Figures 2 and 4; Upchurch et al. 2021: Fig. 2A, 2B, 2C).

In *Hudiesaurus sinojapanorum*, the posterior margins of the postzygapophyses end much anterior to the posterior margin of the centrum, which is also seen in cervical 18 and dorsal 1 of *Xinjiangtitan shanshanesis*, while in dorsal 2 of *Xinjiangtitan shanshanesis*, the posterior margin of postzygapophyses reaches the posterior margin of the centrum. According to the description by Upchurch et al. (2021), the epipophyses are greatly reduced or absent, perhaps replaced by small tab-like process on the postzygapophyses in *Hudiesaurus*. However, in *Xinjiangtitan shanshanesis*, no epipophyses or other processes were detected on the dorsal surface of the postzygapophyses, and most of the dorsal surfaces of the postzygapophyses are covered by the TLP of the trifurcated neural spine. The small tab-like process in *Hudiesaurus sinojapanorum* is just part of the TLP, as seen in Figure 18 from Upchurch et al. (2021). The hyposphene-hypantrum system is recorded in the original description of *Hudiesaurus sinojapanorum* (Dong 1997), but this articulation does not discern by reobservation of the figures in the original article (Figure 17A; Dong 1997: Figs.1 and 3; Upchurch et al. 2021: Fig. 2D), which is replaced by the paired descended separately CPOLs and the 'V' -shaped TPOLs as in *Xinjiangtitan shanshanesis* (Figure 3C). The difference is that CPOLs in *Hudiesaurus sinojapanorum* bifurcate dorsally (Figure

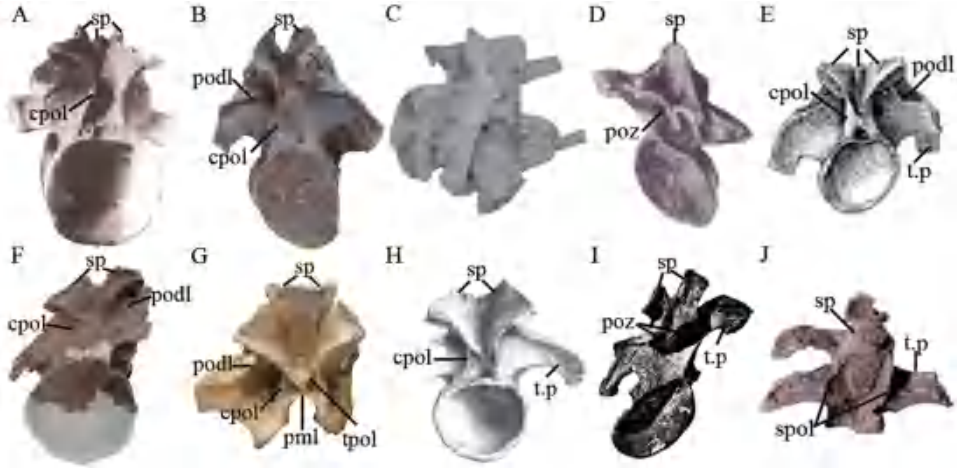

Figure 17. Anterior dorsal vertebrae of *Xinjiangtitan shanshanesis* (SSV12001) and other sauropods. A, posterior view of dorsal 1 of *Hudiesaurus sinojapanorum* (Dong, 1997: Fig.3); B, posterior view of dorsal 2 of *Klamelisaurus gobiensis* (Moore et al., 2020:Fig.8J); C, dorsal view of dorsal 1 of *Qijianglong guokr* (Xing et al., 2015a:Fig.13A); D, posterior view of dorsal 3 of *Omeisaurus tianfuensis* (He et al., 1988: Plate VI.1b); E, posterior view of dorsal 1 of *Euhelopus zydanskyi* (Wiman, 1929: Plate III: fig17); F, posterior view of dorsal 1of *Xinjiangtitan shanshanesis*; G, posterior view of anterior dorsal (?dorsal 1) of *Bellusaurus sui* (Mo et al., 2013: Plate 24B); H, posterior view of dorsal 1of *Mamenchisaurus youngi* (Ouyang and Ye, 2002:Fig.19B); I, posterior view of dorsal 1of *Mamenchisaurus hochuanensis* (Young and Chao, 1972:Plate XII); J, posterodorsal view of dorsals 4-5 of *Omeisaurus puxiani* (Tan et al., 2020:Fig4b). Not to scale.

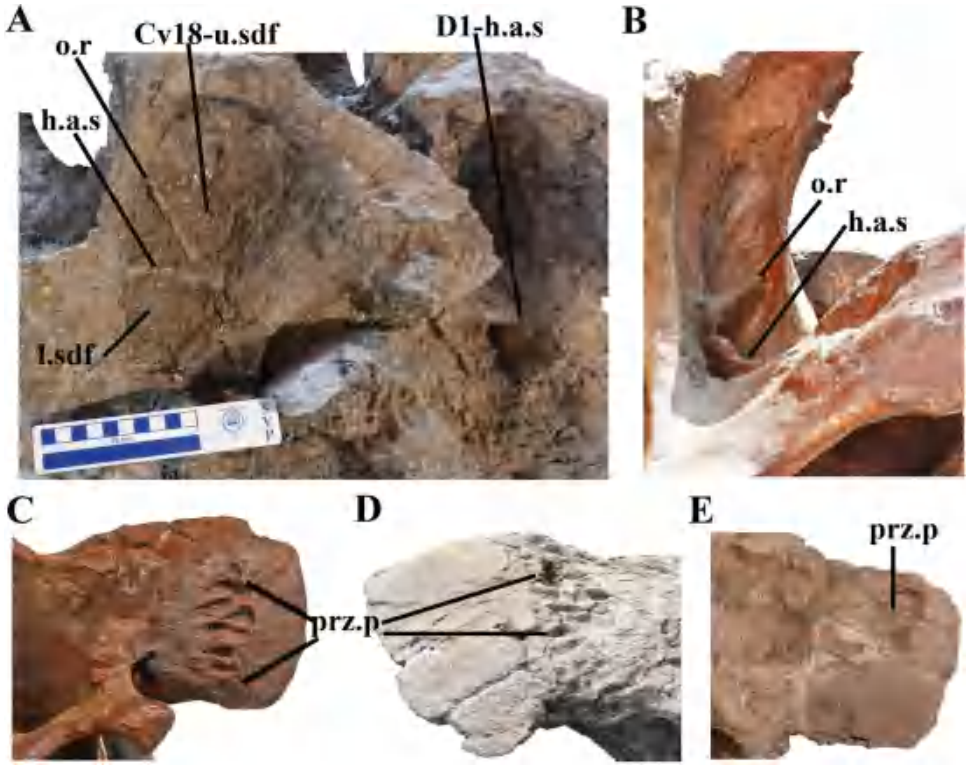

Figure 18. Close-up of cervicodorsal vertebrae of of *Xinjiangtitan shanshanesis* (SSV12001) and *Hudiesaurus sinojapanorum*. A, close-up of left spinodiapophyseal fossa of cervical 18 and dorsal 1 of *Xinjiangtitan shanshanesis*; B, close-up of left spinodiapophyseal fossa of cervicodorsal vertebra of *Hudiesaurus sinojapanorum* (Upchurch et al., 2021: fig.2A); C, close-up of prezygapophysis of cervicodorsal vertebra of *Hudiesaurus sinojapanorum* (Upchurch et al., 2021: fig.3A); D, close-up of prezygapophysis of cervical 18 of *Xinjiangtitan shanshanesis*; E, close-up of prezygapophysis of dorsal 2 of *Xinjiangtitan shanshanesis*. Scale bars: A, 10cm; B-E, not to scale.

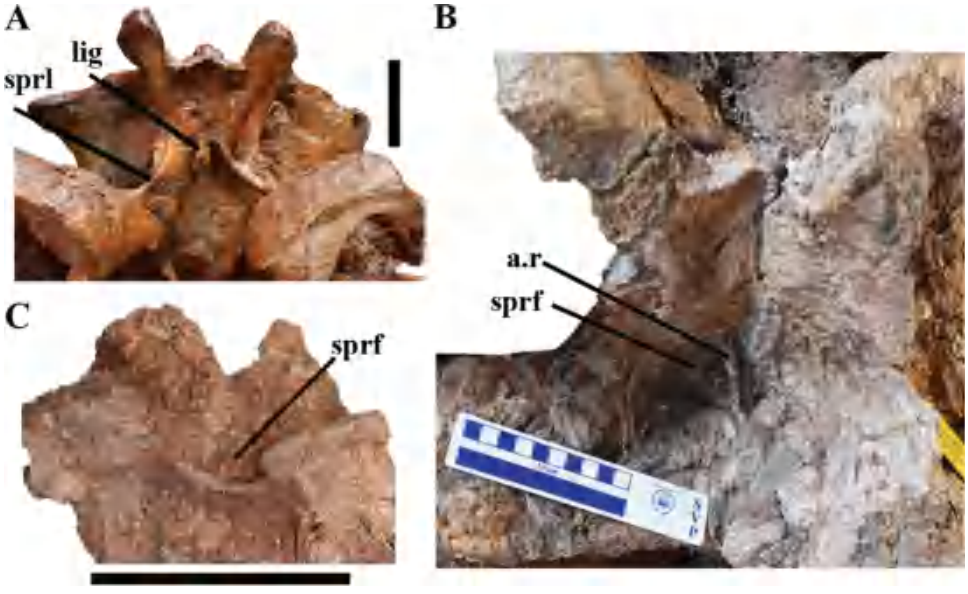

Figure 19. Cervicodorsal vertebrae of *Xinjiangtitan shanshanesis* (SSV12001) and *Hudiesaurus sinojapanorum* in anterior views. A, close-up of the spinoprezygapophyseal laminae of cervicodorsal vertebra of *Hudiesaurus sinojapanorum* (Upchurch et al., 2021: fig.2C); B, close-up of the spinoprezygapophyseal fossa of cervical 18 of *Xinjiangtitan shanshanesis*; C, close-up of the spinoprezygapophyseal fossa of dorsal 2 of *Xinjiangtitan shanshanesis*. Scale bars: A-B, 10cm; C, 30cm.

3C 17A, 17F; Upchruch at al. 2021: Fig. 2C, 2D). Each SPRL in *Hudiesaurus sinojapanorum* splits into two branches, while those of cervical 18 and dorsals 1–2 in *Xinjiangtitan shanshanesis* are present as single laminae (Figure 19A, 19B). The former is regarded as an autapomorphy (Upchurch et al. 2021). Furthermore, there is a large flat space on the anterior surface of the neural spine between the SPRLs and an anteriorly directed laterally compressed sword-like process presents on anterior of neural spine (Dong 1997), which is interpreted to be part of an ossified ligament in *Hudiesaurus sinojapanorum* by re-assessment of *Hudiesaurus*

sinojapanorum (Upchurch et al. 2021). This is not the case with cervical 18 of *Xinjiangtitan shanshanesis*, where has a small deep SPRF between the SPRLs and a short accessory ridge (A.R) within the SPRF, projecting dorsally to the right metapophysis and ventrally to the left prezygapophysis (Figure 19B). The region between the SPRLs of dorsal 1 cannot be identified due to articulated preservation of cervical 18 and dorsal 1 in *Xinjiangtitan shanshanesis*, while there is a shallower SPRF without any ridge in dorsal 2 of *Xinjiangtitan shanshanesis* (Figure 19C). As in cervical 18, dorsal 1 and dorsal 2 of *Xinjiangtitan shanshanesis*, the neural spine is relatively low projecting slightly above the level of the postzygapophyses in *Hudiesaurus sinojapanorum*. However, differently, the posterior margin of the neural spine slopes strongly forward in *Hudiesaurus sinojapanorum*, while that of cervical 18 sloeps strongly posteriorly, those of dorsals 1-2 slope slightly posteriorly in *Xinjiangtitan shanshanesis* (Figures 2 and 3; Dong 1997: Fig.1; Upchruch at al., 2021: Fig.2). The bifurcation of neural spine is also different between the two taxa though they all bifurcate into three parts. In anterior and posterior views, the bifurcation in *Hudiesaurus sinojapanorum* is more like 'W'-shaped with an acute median tubercle directing anteriorly and a pair of dorsoventrally markedly expanded metapophyses in contrast to that of *Xinjiangtitan shanshanesis* (Figures 3C, 17; Upchurch et al. 2021: Fig. 2C, 2D). Each metapophysis in *Xinjiangtitan shanshanesis*, meanwhile, extends posterolaterally to develop a more symmetrical triangular lateral process that overlaps the SPOL. In *Hudiesaurus sinojapanorum*, the metapophyses project posterolaterally as acute laminae with bifurcated ends that are identified as the SPOL. As reobservation of the figures in the original article (Dong 1997: Figs. 1, 2; Upchurch et al. 2021: Fig. 2D), the bifurcation of the SPOL is similar to the TLP of cervical 18 in *Xinjiangtitan shanshanesis*, the SPOLof *Hudiesaurus sinojapanorum* may also be a combination of the SPOL and TLP if it is possible (Figures 3, 6; Upchurch et al. 2021: Figs. 2, 3)

As in cervical 18 of *Xinjiangtitan shanshanesis*, there are two accessory ridges subdivided the SDF in *Hudiesaurus sinojapanorum*, one is an oblique accessory ridge (O.R) and the other one is a horizontal accessory strut (H.A.S). However, the difference is that the horizontal accessory ridge of *Hudiesaurus sinojapanorum* presents as a thick posterior and tapering forwards strut rather than the horizontal ridge in *Xinjiangtitan shanshanesis*. Dorsal 1 of *Xinjiangtitan shanshanesis* lacks the oblique accessory lamina, while exhibits the SPDL in dorsal 2 of *Xinjiangtitan shanshanesis* (Figure 18A, 18B). Compared with cervical 18, dorsal 1 and dorsal 2 of *Xinjiangtitan shanshanesis*, the vertebrae of *Hudiesaurus sinojapanorum* share more similar morphological characteristics with cervical 18 than dorsals 1–2, so it might be the last cervical as that proposed by Upchurch et al. (2021).

Bellusaurus sui

Dong (1990) named a sauropod–*Bellusaurus sui*, which was recovered in the upper beds of Shishugou Formation in Jiangjunmiao and Karamay regions, Xinjiang (Dong 1990; Mo 2013; Moore et al. 2017; Moore et al. 2018). Morre et al. (2018) noted that *Bellusaurus sui* is likely early Late Jurassic in age. *Bellusaurus sui* was proposed as a juvenile form of *Klamelisaurus* (Paul 2010), but Moore et al. (2020) proposed that the two taxa have several differences, which cannot be explained by different ontogenetic stages. Here, we separate it from *Klamelisaurus gobiensis*, and compare them with *Xinjiangtitan shanshanesis,* respectively. The centra and neural arches of all dorsal vertebrae in *Bellusaurus sui* are separately preserved. *Bellusaurus sui* has opisthocoelous dorsal centra as in *Xinjiangtitan shanshanesis*. The ventral surface of dorsal 1 in *Bellusaurus sui* bears a low ridge on the midline, and the ventral surfaces of anterior and middle dorsal centra in *Bellusaurus sui* are transversely convex, bearing weakly developed ventral keels (Mo 2013), but the condition of *Xinjiangtitan shanshanesis* is unknown due to lacking the ventral portion of centra; in preserved dorsal centra of *Xinjiangtitan shanshanesis* (dorsals 8–12), the ventral surfaces are smooth and concave, while those of posterior dorsals in *Bellusaurus sui* are transversely convex (Mo 2013). In *Bellusaurus*, the pleurocoels of centrum extend nearly to the midline of the centrum, but those of *Xinjiangtitan shanshanensis* are restricted to the anterodorsal portion of the dorsal centra. The postzygapophyses of the anterior dorsal vertebrae of *Bellusaurus sui* meet each other medially to produce the intrapostzygapophyseal lamina (TPOL), and the laminae are fused to mark the dorsal limit of a short vertical posterior midline lamina (PML) (Figure 17C). In contrast to *Bellusaurus sui*, the postzygapophyses of dorsal 1 in *Xinjiangtitan shanshanesis* do not meet each other so that the TPOL and the PML are not developed. The postzygapophyses of other anterior dorsal vertebrae of *Xinjiangtitan shanshanesis*, meanwhile, connect each other but form the hyposphene-hypantrum system rather than the TPOL and the PML. A lateral centropostzygapophyseal lamina (L. CPOL) projects above the embayed posterior surface, incompletely dividing the POCDF into posterior dorsal vertebrae of *Bellusaurus*; unlike the condition in *Bellusaurus sui*, the lateral CPOL positions on the same flat surface under the postzygapophysis of dorsal 9 in *Xinjiangtitan shanshanensis* (Figure 20B, 20C). A dorsally bifurcated SPDL in the middle and posterior dorsal vertebrae and the anterior and posterior branches extend entirely to the SPRL and SPOL in *Bellusaurus sui*, whereas in middle and posterior dorsals of *Xinjiangtitan*, the dorsally bifurcated SPDL is the M. SPDL, and the anterior branch extend dorsally to the SPRL, while the posterior branch did not contract the SPOL.

Bellusaurus sui still differs from *Xinjiangtitan shanshanesis* in that: sharing unbifurcated neural spines (Figure 17G); having a deep, sharp-lipped pneumatic fossa in posterior dorsal centra and a vertical accessory strut within the pneumatic fossa (Mo 2013: Plate 30E); lacking the A. SPOL, the M. SPDL, and the P. SPOL in dorsal series; presence of dual ridges on the proximal anterior surface of dorsal rib without the pneumatic fossa (PF) placed at the base of the acute ridge.

Klamelisaurus gobiensis

Klamelisaurus gobiensis was first reported by Zhao (1993). *Klamelisaurus gobiensis* was recovered from the lower beds of the Shishugou Formation in the eastern Junggar Basin, Xinjiang (Zhao 1993; Li et al. 2011; Moore et al. 2020). According to redescription of *Klamelisaurus gobiensis* by Moore et al. (2020), they have several similarities in laminae and fossae construction: deep and undivided pleurocoel with acute posterior margin in first two dorsal centra, a dorsally bifurcated SPDL (bif.SPDL) in middle dorsal vertebrae (Figure 21). The latter was considered the unique autapomorphy (Moore et al. 2020). However, in addition to the bifurcated SPDL, the dorsal 4 of *Xinjiangtitan shanshanensis* also has a posterior SPDL (P.SPDL) that is absent in *Klamelisaurus gobiensis* (Figure 21). The differences between them are remarkable. For example, dorsal centra in *Klamelisaurus gobiensis* are shorter anteroposteriorly with elliptic posterior concave (higher than wide), while the anterior and posterior articular surfaces of centrum in *Xinjiangtitan shanshanensis* are subcircular. The ventral surfaces of dorsals 1–7 in *Klamelisaurus gobiensis* bear low ventral ridge (Moore etal. 2020), while the condition of *Xinjiangtitan shanshanesis* is unknown due to reconstruction of the ventral portion of centra in dorsals 8–12 of *Xinjiangtitan shanshanesis*, the ventral surfaces are smooth and

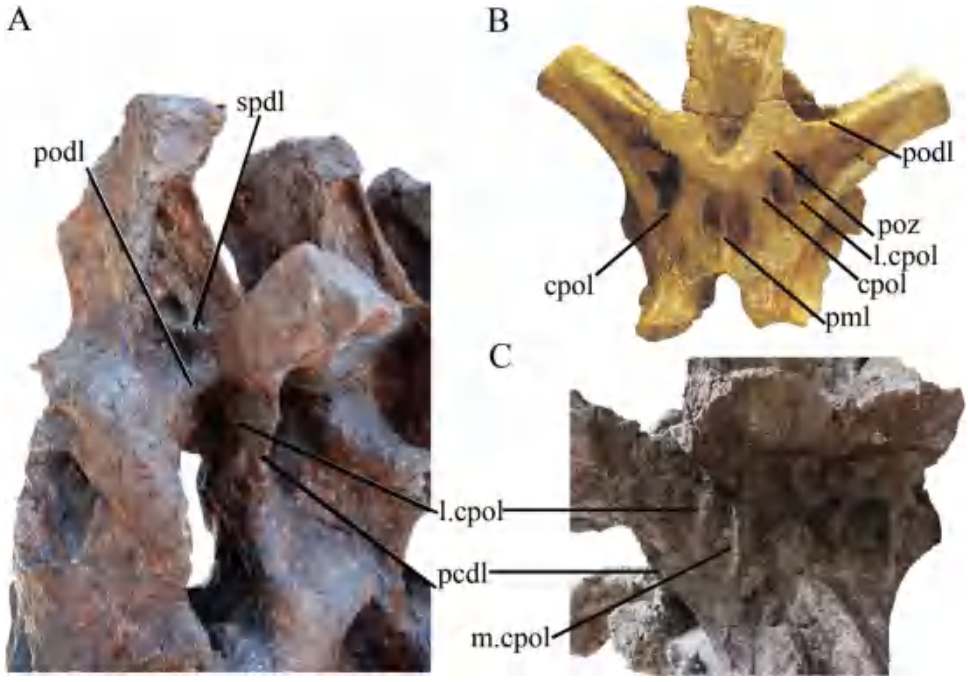

Figure 20. Lateral centropostzygapophyseal lamina in posterior dorsal vertebrae of *Xinjiangtitan shanshanesis* (SSV12001) and other sauropods. A, right posterolateral view of dorsal 7 of *Klamelisaurus gobiensis* (IVPP V9492) (Moore et al. 2020: Fig. 13A), posterior view of a posterior dorsal neural arch of *Bellusaurus sui* (IVPP V17768.95) (Mo 2013: Plate31B). C, posterior view of dorsal 9 of *Xinjiangtitan shanshanesis* (SSV12001). Not to scale.

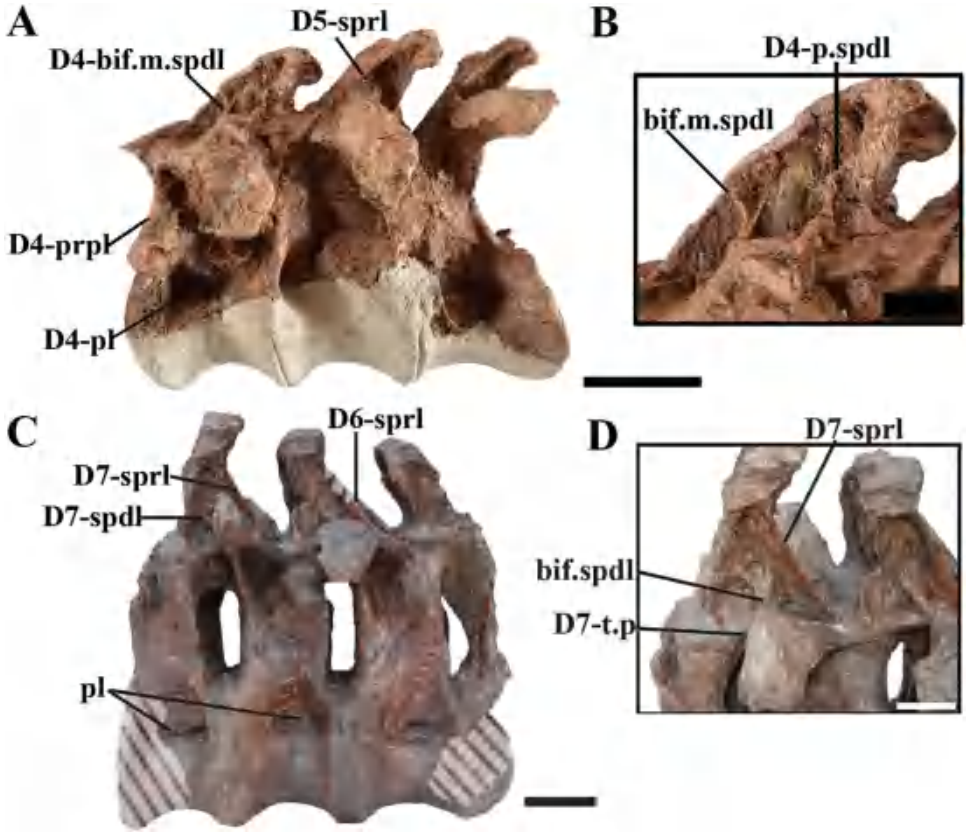

Figure 21. Middle dorsal vertebrae of *Xinjiangtitan shanshanesis* (SSV12001) and *Klamelisaurus gobiensis* (IVPP V9492). A, left lateral view of dorsals 4–6 of *Xinjiangtitan shanshanesis*; B, close-up of bifurcated spinodiapophyseal lamina of dorsal 4 of *Xinjiangtitan shanshanesis*; C, right lateral view of dorsals 5–8 of *Klamelisaurus gobiensis* (Moore et al. 2020: Fig. 10C) close-up of bifurcated spinodiapophyseal lamina of dorsal 7 of *Klamelisaurus gobiensis* (Moore et al. 2020: Fig. 10G). Scale bars: A, 30 cm; B, 10 cm; C, 10 cm; D, 5 cm.

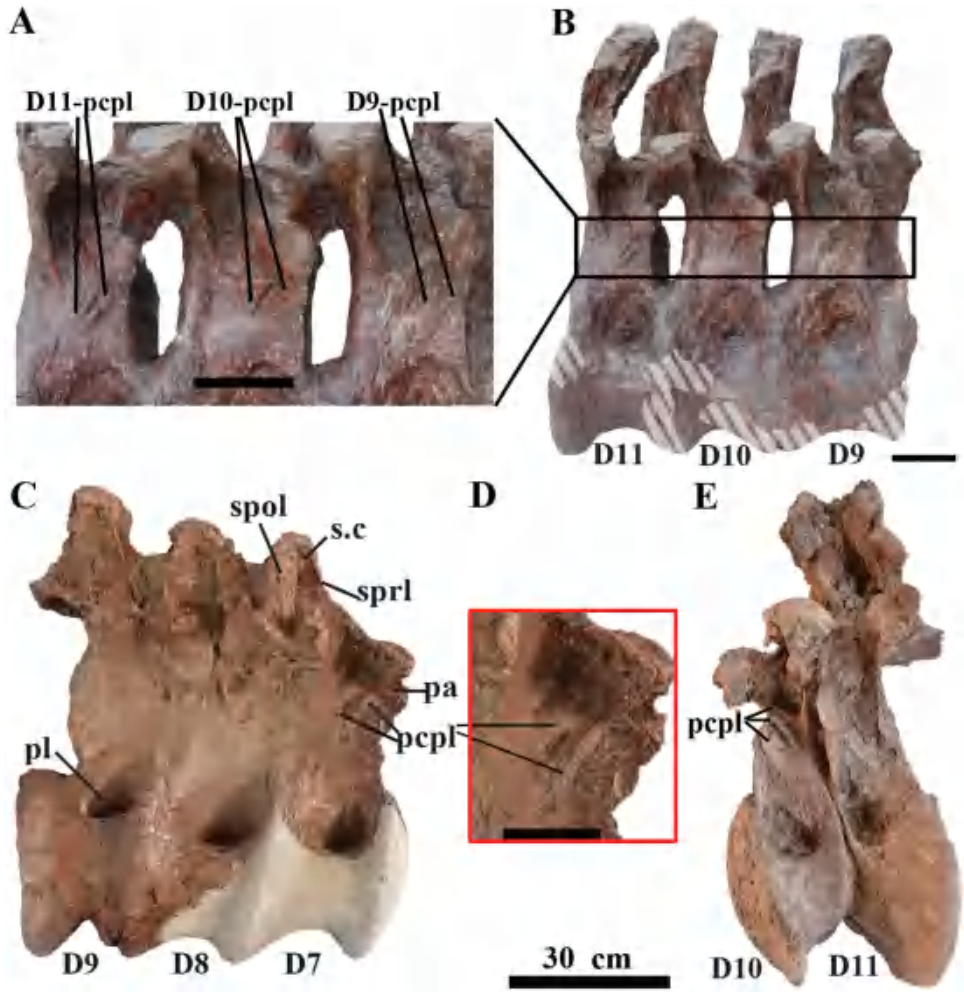

Figure 22. Posterior centroparapophyseal laminae in middle-posterior dorsal vertebrae of *Klamelisaurus gobiensis* (IVPP V9492) and *Xinjiangtitan shanshanesis* (SSV12001). A, close-up of the PCPLs in dorsals 9–11 of *Klamelisaurus gobiensis* in right view (Moore et al. 2020: Fig. 11c) dorsals 9–11 of *Klamelisaurus gobiensis* in right view (Moore et al. 2020: Fig. 11C) dorsals 7–9 of *Xinjiangtitan shanshanesis* in right view; D, close-up of the PCPLs in dorsal 7 of *Xinjiangtitan shanshanesis* in right view; E, dorsals 10–11 of *Xinjiangtitan shanshanesis* in left view. Scale bars: A-B, 10 cm; C, E, 30 cm; D, 10 cm.

concave, but in *Klamelisaurus*, the ventral ridge is absent in dorsal 8 and dorsal 12 and unknown in dorsals 9–11. The middle dorsal neural arch (dorsals 4–7) of *Klamelisaurus gobiensis* is relatively upright (Figure 19A, 19C), the maximum height of the dorsal vertebra is much lower. The smaller and shallower pleurocoels of *Klamelisaurus gobiensis* position on mid-dorsal portion of the centra with a posteriorly acute almond-shaped pneumatic foramen, while in *Xinjiangtitan shanshanensis*, there is no pneumatic foramen in the deep pleurocoels, located in most-anterodorsal portion of centra with acute anterior and ventral boundary (Figure 21A, 21C). A very low, vertically orientated incipient lateral branch of the CPOL descends from the postzygapophysis to the halfway to the ventral edge of the PCDL, incompletely dividing the POCDF into dorsal 7 of *Klamelisaurus gobiensis*. This structure is unlike the condition in *Xinjiangtitan shanshanensis*, in which the lateral CPOL projects lateroventrally as a distinct lamina (Figure 20A, 20C). In *Xinjiangtitan shanshanensis*, there is a horizontal accessory strut subdividing the SDF in dorsals 1–2, while the accessory strut is only present in dorsal 1 in *Klamelisaurus gobiensis*. As in *Xinjiangtitan*, neural spine bifurcation persists through dorsals 1-5 with metapophyses and the lateral triangular processes in *Klamelisaurus gobiensis*. Although only dorsal 1 shares a small bump according to Moore er al.(2020) that is corresponding to the median tubercle of bifurcated neural spine in *Xinjiangtitan shanshanensis*, by reobserving the figures from Moore et al. (2020), the median tubercle presents in the bifurcation of neural spines of dorsals 1-8 in *Klamelisaurus*, which is similar to the bifurcation of the neural spines of dorsals 1–9 in *Xinjiangtitan* (Moore et al. 2020: Figs. 8 I, 9G, 10E); the metapophyses of bifurcated neural spines of *Klamelisaurus* are better developed than those in *Xinjiangtitan*; the lateral triangular processes of the neural spine present as dorsolaterally facing platform in *Klamelisaurus*, while that of *Xinjiangtitan* faces dorsally; furthermore, the lateral triangular processes on both sides extend far more laterally than that of *Klamelisaurus* (Figure 23); in posterior view, the bifurcation area presents as a 'W'-shaped cleft in *Xinjiangtitan*, whereas that is 'V'-shaped and shallow 'U'-shaped clefts in *Klamelisaurus* (Figure 17B). The non-bifurcated neural spines (dorsals 9–12) in *Klamelisaurus gobiensis* areangled slightly anteriorly rather than posteriorly in that of *Xinjiangtitan shanshanensis* (Figure 20A, 20). *Klamelisaurus* share triplicate PCPLs in some posterior dorsal vertebrae, while in *Xinjiangtitan*, there are bipartite or triplicate PCPLs in some middle-posterior dorsal vertebrae (Figure 22). Apart from that, *Klamelisaurus gobiensis* can be distinguished from *Xinjiangtitan shanshanensis* in having a ventral keel in dorsals 3–7, shorter transverse process projecting horizontally in anterior dorsal vertebrae, and dual ridges on the proximal anterior surface of dorsal rib without the pneumatic fossa (PF).

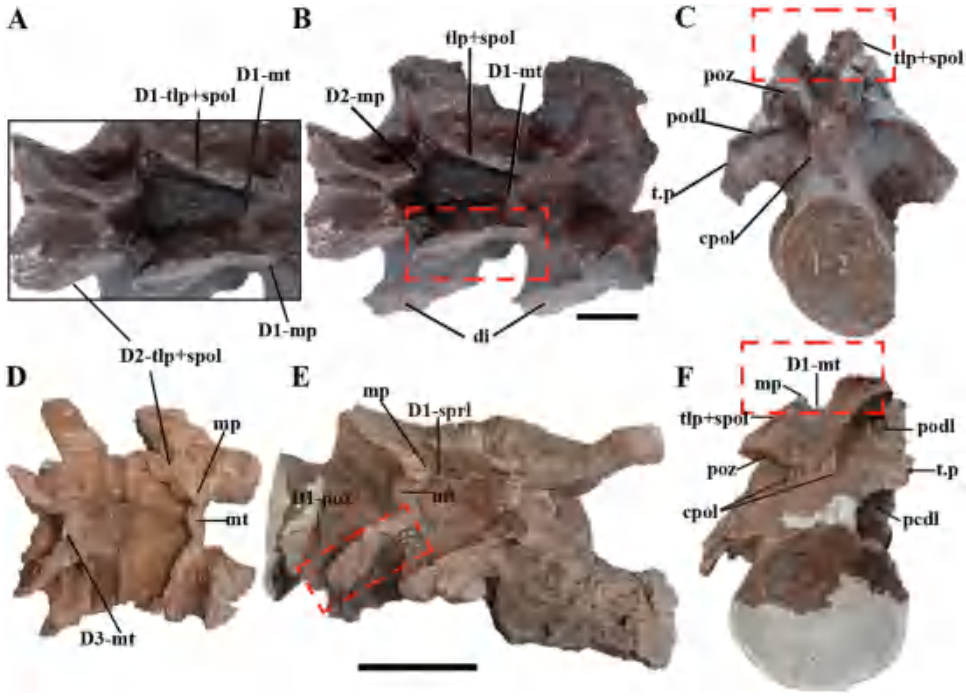

Figure 23. Neural spines in anterior dorsal vertebrae of *Klamelisaurus gobiensis* (IVPP V9492) and *Xinjiangtitan shanshanesis* (SSV12001). A, close-up of the neural spines in dorsals 1–2 of *Klamelisaurus gobiensis* in dorsal view (Moore et al. 2020: Fig. 8J) neural spines in dorsals 1–2 of *Klamelisaurus gobiensis* in dorsal view (Moore et al. 2020: Figure. 8jJ) neural spines in dorsals 1–2 of *Klamelisaurus gobiensis* in posterior view (Moore et al. 2020: Figure. 8jJ) neural spines in dorsals 2–3 of *Xinjiangtitan shanshanesis* in dorsal view; E, neural spines in cervical 18 and dorsal 1 of *Xinjiangtitan shanshanesis* in dorsal view; F, neural spines in cervical 18 and dorsal 1 of *Xinjiangtitan shanshanesis* in posterior view. Scale bars: A, not to scale; B-C, 10 cm; D-F, 30 cm.

Euhelopus zdanskyi

Euhelopus zdanskyi was collected from grey sandstone deposits of Mengyin Formation in Shandong Province (Wiman 1929; Wilson and Upchurch 2009). The evolutionary relationship of *Euhelopus zdanskyi* and Mamenchisaurids has been controversial for a long time (Wilson and Sereno 1998; Wilson 2002; Moore et al. 2020). The different geological ages of *Euhelopus zdanskyi* and *Xinjiangtitan shanshanensis* imply taxonomic separation, as *Euhelopus zdanskyi* is from Early Cretaceous of Mengyin Formation. Based on the redescription of *Euhelopus zdanskyi* by Wilson and Upchurch (2009), here, we mainly compare example a (PMU 233), example b (PMU234) and of *Euhelopus zdanskyi* with *Xinjiangtitan shanshanensis*. Example a consists anterior and posterior dorsal vertebrae; example b consists only the posterior dorsal vertebrae (Wilson and Upchurch 2009). In general, the anteroposteriorly elongated pleurocoels of dorsal vertebrae in *Euhelopus zdanskyi* (PMU 233, PMU 234) present as dorsally defined shallow fossae in the dorsal portion of centra, while the pleurocoels of *Xinjiangtitan shanshanensis* are much deeper and smaller without clear dorsal boundary, located at anterodorsal portion of the centra. The first four dorsal centra of *Euhelopus zdanskyi* (PMU 233) have dorsally sharply defined pleurocoels, while the pleurocoels of the first two dorsals in *Xinjiangtitan shanshanensis* merge with the CDF dorsally without the defined dorsal margin. The transverse processes are pendants with flattened lateral surfaces in anterior dorsals of *Euhelopus zdanskyi* (PMU 233), as that in *Xinjiangtitan shanshanensis*. The ACPL firstly appears in dorsal 5 in *Euhelopus zdanskyi* (PMU 233), whereas that presents firstly in dorsal 7 in *Xinjiangtitan shanshanensis* (Figure 9B; Wilson and Upchurch 2009: Fig.16). Camellate pneumaticity appears in dorsal vertebrae of *Euhelopus zdanskyi* (dorsal 7 PMU 233) (dorsal 10 PMU 234), which also appears in dorsal 10 in *Xinjiangtitan shanshanensis* (Figure 12 A, 12E; 12 and Upchurch 12: Fig.12)

Zhang et al. (2020) reported that *Xinjiangtitan shanshanensis* shared several important features of the cervical series with *Euhelopus zdanskyi*, such as the horizontal accessory strut (EPRL, Wilson and Upchurch 2009) separating two pneumatocoels in cervical vertebrae, bifurcated neural spine with medial tubercle. The horizontal accessory strut (remnant of the EPRL, Wilson and Upchurch 2009) continues to present in dorsals 1–2 of *Euhelopus zdanskyi* (PMU 233), and it is replaced by the SPDL in dorsal 3. This condition is also present in dorsals of *Xinjiangtitan shanshanesis*. The anterior dorsal neural spines bifurcate with medial tubercle, but the median tubercles of the bifurcated dorsal spines in *Euhelopus zdanskyi* are as large as or larger (dorsoventrally taller) than metapophyses, whereas those of *Xinjiangtitan shanshanensis* are smaller and lower than metapophyses (Figure 17E, 17F). Furthermore, bifurcation of spine is broader with transversely wider TLP than that in *Euhelopus zdanskyi* (Figures 3, 6; Wilson and Upchurch 2009: Fig.15). The PCDL, the PCPL and the ACDL of the middle and posterior dorsals cross to form 'K' configuration in *Euhelopus zdanskyi* (PMU 233) (Wilson and Upchurch 2009), but the middle and posterior dorsal vertebrae of *Xinjiangtitan shanshanensis* lack the 'K' configuration. *Euhelopus zdanskyi* dorsals lack the sloping secondary crests (S.C) situated at the dorsal end of the SDF, which is observed in dorsals 4–6 of *Xinjiangtitan shanshanensis* (Figure 7D, 7E). In *Euhelopus zdanskyi* (PMU 233), the SPDLs of the anterior dorsals are slightly forwardly orientated or vertically shown from the figure of the original paper (Wilson and Upchurch 2009: Fig. 17) though Wilson and Upchurch (2009) said they were vertical. A different condition presents in *Xinjiangtitan shanshanensis*, where the L. SPDL and the M. SPDL

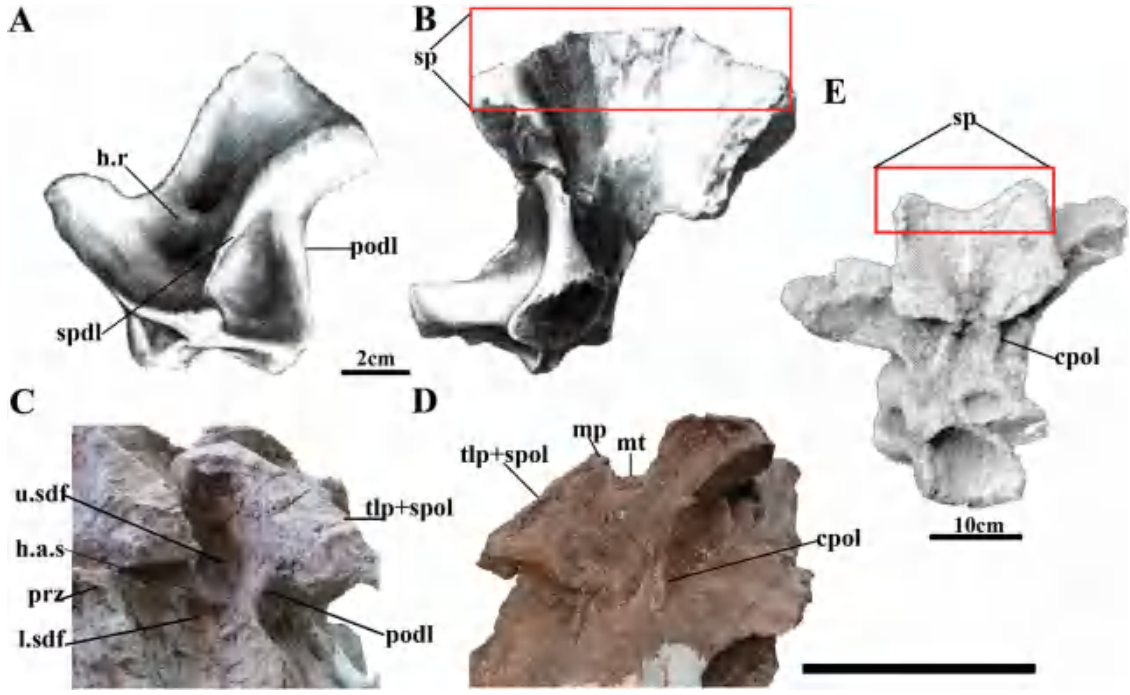

Figure 24. Dorsal 1 of *Daanosaurus zhangi* (ZDM 0193), *Xinjiangtitan shanshanesis* (SSV12001) *Dashanpusaurus dongi* (ZDM 5028). A, close-up of the spinodiapophyseal fossa in dorsal 1 of *Daanosaurus zhangi* in left lateral view (Ye et al. 2005: Fig. 4A) close-up of the spinodiapophyseal fossa in dorsal 1 of *Daanosaurus zhangi* in posterior view (Ye et al. 2005: Fig. 4B); C, close-up of the spinodiapophyseal fossa in dorsal 1 of *Xinjiangtitan shanshanesis* in left lateral view; D, close-up of the spinodiapophyseal fossa in dorsal 1 of *Xinjiangtitan shanshanesis* in posterior view; E, dorsal 1 of *Dashanpusaurus dongi* in posterior view (Peng et al. 2005). Scale bars: A-B, 2 cm; C-D, 30 cm; E, 10 cm.

present in the anterior and middle dorsal vertebrae, but the laminae are absent in posterior dorsal vertebrae.

Tienshanosaurus chitaiensis

Tienshanosaurus chitaiensis was recovered from gently dipping, green-yellow sandstone in the upper portion of Shishugou Formation (Young 1937; Dong 1992; Moore et al. 2018). The specimens of *Tienshanosaurus chitaiensis* are represented by two sets of fossils (field number 40002 and 40003) (Young 1937). Young (1937) first reported *Tienshanosaurus chitaiensis* and proposed it had a close affinity to *Euhelopus zdanskyi*. Li (1998) suggested that *Tienshanosaurus chitaiensis* belonged to Mamenchisauridae. Moore et al. (2020) proposed that *Tienshanosaurus* positioned as a close outgroup of 'Core *Mamenchisaurus*-like Taxa'. Therefore, we compared *Tienshanosaurus chitaiensis* and *Xinjiangtitan shanshanesis* even though the elements of *Tienshanosaurus chitaiensis* are not well preserved.

In *Tienshanosaurus chitaiensis* (40002), the neural spines are not bifurcated and oriented slightly posteriorly, the neural arches elongate dorsoventrally, the transverse processes elevate adjacent to the zygapophyses; therefore, we infer that the vertebrae may be the mid-posterior dorsals. As in the middle dorsals of *Xinjiangtitan*, there is a M. SPDL that sundivided the SDF into an anterior SDF and a posterior SDF in preserved dorsals (Young 1937: Fig. 1B), while in *Xinjiangtitan*, the A. SPDL presents in dorsal 3 and the P. SPDL presents in dorsal 4. Given that the right side of vertebrae of *Tienshanosaurus* in good condition and similar to that of *Euhelopus zdanskyi* in original description (Young 1937) we suspect that the 'Fig. 2A' from Young (1937) was miswritten as a left view, which may be a right lateral view. If 'Fig. 2A' (Young 1937) is a right lateral view, the dorsal vertebrae of *Tienshanosaurus chitaiensis* (40002) are opisthocoelous or amphicoelous, the posterior cotyles of the centra are much shallower than those in *Xinjiangtitan shanshanesis*. However, Li (1998) proposed that the dorsals of *Tienshanosaurus* are amphicoelous, the condition is different from *Xinjiangtitan* and other mamenchisaurid sauropods (e.g. *Mamenchisaurus youngi* Ouyang and Ye 2002; *Mamenchisaurus hochunaensis* Yang and Chao 1972; Dong et al. 1983; *Qijianglong* Xing et al. 2015a; *Omeisaurus tianfuensis* He et al. 1988). Furthermore, the pleurocoels of *Tienshanosaurus chitaiensis* are shallower and more anteroposteriorly elongated than those of *Xinjiangtitan shanshanesis*, and located at the mid-dorsal portions of the centra rather than the anterodorsal parts of the centra in *Xinjiangtitan* (Figures 9, 10, 12)

Mamenchisaurus youngi

Mamenchisaurus youngi (Pi et al. 1996; Ouyang and Ye 2002) was unearthed from the Upper Shaximiao Formation in Sichuan Province (Ouyang and Ye 2002). In *Mamenchisaurus youngi*, the middle and posterior dorsal centra have camellate pneumaticity, but that is only present in posterior dorsal centra of *Xinjiangtitan shanshanesis*. In *Xinjiangtitan shanshanesis*, the neural spines of the anterior and middle dorsal vertebrae project posterodorsally bifurcated into three parts with a medial tubercle, the paired metapophyses and the lateral triangular processes, unlike the condition in *Mamenchisaurus youngi*, in which the corresponding neural spine project subvertical, only the first four neural spines are bifurcated with slightly developed medial tubercle and well-developed metapophyses, the latter expand dorsoventrally and project posterolaterally to connect the postzygapophyses as acute laminae rather than flat broad laminae (Ouyang and Ye 2002: Figs 19–21). Unlike *Xinjiangtitan shanshanesis*, the first two dorsal vertebrae of

Mamenchisaurus youngi have shallower and smaller pleurocoels, well-developed intraprezygapophyseal laminae (TPRL) and intrapostzygapophyseal laminae (TPOL) (Figure 17H), but lack the M. SPOL. Compared to the SDF, *Mamenchisaurus youngi* lacks the horizontal accessory strut in dorsals 1–2, the SPDL is located at the slightly posterior portion of the SDF in dorsal 3 rather than the A. SPDL and the M. SPDL in *Xinjiangtitan*. Furthermore, the L. CPOL is not present in the posterior dorsal vertebrae of *Mamenchisaurus youngi* fromthe original description and pictures (Pi et al. 1996; Ouyang and Ye 2002), which is present in *Xinjiangtitan shanshanesis, Hudiesaurus sinojapanorum, Bellusaurus sui* and *Klamelisaurus gobiensis* (Moore et al. 2018; Moore et al. 2020; Upchurch et al. 2021).

Mamenchisaurus hochuanensis

Mamenchisaurus hochuanensis was discovered from the Upper Shaximiao Formation in the Sichuan Basin (Young and Chao 1972). As in *Xinjiangtitan shanshanesis, Mamenchisaurus hochuanensis* (Young and Chao 1972; Dong et al. 1983) has 12 opisthocoelous dorsal vertebrae; the parapophysis of dorsal 3 to subsequently is completely on the neural arch. There are several differences between them though the deformed material and simplistic description. The anterior faces of the dorsal neural arches of *Mamenchisaurus hochuanensis* are more deeply excavated than that of *Xinjiangtitan shanshanesis*. The hyposphene-hypantrum system presents in the middle and posterior dorsal vertebrae of *Mamenchisaurus hochuanensis*, while that is developed in dorsals 3–7 of *Xinjiangtitan shanshanesis* with the 'Y'-shaped hypantrum in dorsal 4 anda single vertical hypantrum in dorsal 7. The first four dorsal neural spines bifurcate deeply as a 'V'-shaped cleft in *Mamenchisaurus hochuanensis* similar to that of *Klamelisaurus gobiensis*. The spine of dorsal 1 in *Mamenchisaurus hochuanensis* is flat and blunt with a medial shallow groove (Figure 17I); however, in *Xinjiangtitan shanshanesis*, only the neural spines of dorsals 10–12 are not bifurcated, and the bifurcation of the first six dorsal neural spines with a developed medial tubercle appear as 'W'-shaped, the degree of bifurcation gradually decreases from dorsal 7 to dorsal 9.

Daanosaurus zhangi

Daanosaurus zhangi (ZDM 0193 Peng et al. 2005; Ye et al. 2005) has more than 20 presacral vertebrae but in poor preservation. Similar to *Xinjiangtitan*, dorsal centra of *Daanosaurus* are opisthocoelous. There is a SPDL dividing the SDF of dorsal 1 into anterior and posterior portions as that of dorsal 3 in *Xinjiangtitan*, but there is another horizontal accessory ridge (H.R) subdivided the anterior portion of the SDF, which also differs from the horizontal accessory strut of dorsals 1–2 in *Xinjiangtitan* (Figure 24A, 24B, 24C, 24D). Moreover, the top of the neural spines of the anterior dorsals in *Daanosaurus* is flat and not bifurcated rather than 'trifid' spines of anterior dorsals in *Xinjiangtitan*.

Dashanpusaurus dongi

Dashanpusaurus dongi (Peng et al. 2005) is from Lower Shaximiao Formation in Sichuan basin. Both the holotype (ZDM 5028) and paratype (ZDM 5027) of *Dashanpusaurus* are preserved 12 dorsal vertebrae, but Peng et al. (2005) believed that it may have 13 dorsal vertebrae. Ren et al. (2022) redescribed *Dashanpusaurus dongi* and proposed that *Dashanpusaurus dongi* is an early-diverging macronarian (Ren et al. 2022). Differ from *Xinjiangtitan*, the anterior dorsal centra are amphiplatyan, the middle dorsal centra are amphiplatyan or weakly amphicoelous and the posterior dorsal centra are weakly amphicoelous in *Dashanpusaurus*; the neural spines of the anterior dorsals of *Dashanpusaurus* weakly bifurcate into shallow 'U'-shaped (Figure 24E; Peng et al. 2005: Fig.61) or wide 'V'-shaped (Ren et al. 2022 : Fig. 7I); the dorsally bifurcated SPDL, A.SPDL, P. SPDL and dorsally bifurcated SPRL are absent in dorsals of *Dashanpusaurus*. The CPOL of dorsal 1 of *Dashanpusaurus* is more developed than that in *Xinjiangtitan*. The ratio of the length of the first dorsal vertebra to the length of the last cervical vertebra of *Dashanpusaurus* is 0.60 (Peng et al. 2005), while that of *Xinjiangtitan* is 0.53. Furthermore, the epipophyses are situated at the posterior portion of the postzygapophyses of the anterior dorsal vertebrae (Ren et al. 2022), while that are absent in dorsal vertebrae of *Xinjiangtitan*. As in *Xinjiangtitan*, there is no SPDL sundividing the SDF in first two dorsals of *Dashanpusaurus*, but differently, *Dashanpusaurus* lacks the horizontal accessory strut that subdivided the SDF of dorsals 1-2 of *Xinjiangtitan*. The L.SPOL and the M.SPOL present in middle dorsals of *Dashanpusaurus* (Ren et al. 2022: Figs.10B, 11B), this condition resembles that of *Xinjiangtitan*, in which there are L.SPOL, M.SPOL and a shallow SPOL-F in dorsals 3-11.

Mamenchisaurus anyuensis

Mamenchisaurus anyuensis was reported in 1996 (He et al. 1996), whose holotype (AL001) includes a complete dorsal column. As in *Xinjiangtitan shanshanesis, Mamenchisaurus anyuensis* bears 12 dorsal vertebrae articulated with the most posterior cervical vertebrae, and all the centra are opisthocoelous with typical pleurocoels (He et al. 1996: Fig. 1); the first six dorsal neural spines are bifid; the hyposphene-hypantrum system appears from dorsal 3 to succeeding dorsals (He et al. 1996; Li 2012). However, *Mamenchisaurus anyuensis* differs from *Xinjiangtitan shanshanesis* in that the anterior dorsal neural spines of *Mamenchisaurus anyuensis* are extremely weakly bifid, and the middle dorsal neural spines of *Mamenchisaurus anyuensis* are not bifurcated; l the middle and posterior dorsals do not have the M. SPOL, the M. SPDL and two nearly parallel CPOLs. Given the simple original description and blurred figures, it is difficult to make further comparison between the two taxa.

Qijianglong guokr

Qijianglong guokr (Xing et al. 2015a) was unearthed from Upper Jurassic Suining Formation in Sichuan Basin. By re-examination of the cervical vertebrae of *Xinjiangtitan shanshanesis* (Zhang et al. 2020), the cervical vertebrae are similar to that of *Qijianglong guokr*, such as a finger-like process above the postzygapophysis exceeding the postzygapophysis posteriorly and the the remant epipophyseal-prezygapophyseal lamina subdividing the SDF.

Only six anterior dorsal vertebrae are preserved poorly in *Qijianglong guokr* (Xing et al. 2015a: Fig. 13). Although the preservation of *Qijianglong guokr* makes comparison difficult, there are several differences between the two taxa (Figure 17C). The prezygapophyseal centrodiapophyseal fossae (PRCDF) of dorsals 3–6 of *Qijianglong guokr* have four distinct pneumatopores, whereas in *Xinjiangtitan shanshanesis*, the PRCDF of dorsal 3 lacks these pneumatopores; moreover, the fossae and laminae in dorsals 4–6 become more complex, the PRCDF is divided into the PRPADF and the parapophyseal centroprezygapophyseal fossa (PACPRF) by the PRPL (Figure 7A). The postzygapophyseal centrodiapophyseal fossa (POCDF) occupies about three times the area of the PRCDF in lateral view in dorsal 5 of *Qijianglong guokr* (Xing et al. 2015a: Fig. 13D), but the POCDF is not developed in dorsals 4–6 of *Xinjiangtitan shanshanesis*.

Xinjiangtitan shanshanesis bears the hyposphene-hypantrum system on dorsal vertebrae from dorsal 3 to dorsal 7, but that is unclear in *Qijianglong guokr* (Xing et al. 2015a); the dorsal neural arches with the spines in *Qijianglong guokr* are at least 1.5 times the height of the centra, but the ratio of *Xinjiangtitan shanshanesis* is smaller (the minimum of the ratio of dorsal 10 in *Xinjiangtitan* is 1.1). It indicates that the neural arches and spines of *Qijianglong guokr* are more dorsoventrally elongated than that of *Xinjiangtitan shanshanensis*; the bifurcated dorsal spines of *Qijianglong guokr* differ from *Xinjiangtitan shanshanesis* in lacking the medial tubercle and the triangular lateral processes.

Omeisaurus tianfuensis

Omeisaurus tianfuensis (He et al. 1988) was discovered in the Lower Shaximiao Formation of the Sichuan Basin, whose holotype (T5701) and paratype (T5704) both have 12 dorsal vertebrae in good preservation (He et al. 1988). As in *Xinjiangtitan shanshanesis*, the dorsal centra of *Omeisaurus tianfuensis* are opisthocoelous, and the hyposphene-hypantrum system is absent in dorsals 1–2. However, unlike *Xinjiangtitan shanshanesis*, the pleurocoel is not well developed in first dorsal in *Omeisaurus tianfuensis*, and the cross section of dorsal centrum has a honeycomb structure that is absent in other dorsal vertebrae. Furthermore, all the dorsal neural spines of *Omeisaurus tianfuensis* are not bifurcated (Figure 17D) in contrast to the bifurcated anterior and middle dorsal neural spines of *Xinjiangtitan shanshanesis*. It still differs from *Xinjiangtitan shanshanesis* as follows: the SPDL is weakly developed in the middle dorsal vertebrae lacking the M. SPDL and the L. SPDL; the SPOLs of dorsals 4–12 appear as posteriorly extending flange; the neural spines of dorsals 11–12 significantly slopes posteriorly.

Omeisaurus puxiani

Omeisaurus puxiani (CLGRP V00005) (Tan et al. 2020) was unearthed from the lower to middle portion of the lower member of the Shaximiao Formation including 12 dorsal vertebrae. As in *Xinjiangtitan shanshanesis*, the internal pneumaticity is present in dorsal centra of *Omeisaurus puxiani*. Tan et al. (2020) proposed the diagnoses of dorsals of *Omeisaurus puxiani* as follows: lateral fossae of dorsal centra are divided by secondary septa, while the pleurocoels of dorsal centra of *Xinjiangtitan shanshanesis* are single; dorsal neural spine ends are knob-shaped and the neural spines of posterior dorsals are transversely extended, in contrast to bifurcated neural spines with a medial tubercle in *Xinjiangtitan shanshanesis*. Furthermore, the SPOLs present as posteriorly extended flange in all dorsal vertebrae of *Omeisaurus puxiani* (Figure 17J), unlike the condition in *Xinjiangtitan shanshanesis*, in which the neural spines of the first two dorsal vertebrae merge with the TLP of neural spines, and the stout M. SPOL and the thin L. SPOL are developed in the rest of the dorsals.

Chuanjiesaurus anaensis

Chuanjiesaurus anaensis (Fang et al. 2000; Sekiya 2011) was first named by Fang et al. (2000) from Middle Jurassic Chuanjie Formation in Lufeng County. Sekiya (2011) re-evaluated the holotype and a referred specimen, considered *Chuanjiesaurus anaensis* as a member of Mamenchisauridae. The dorsal vertebrae were not preserved in the holotype of *Chuanjiesaurus anaensis*, while the referred specomen (LCD9701-I) has at least seven posterior dorsals (Sekiya 2011). As in *Xinjiangtitan shanshanesis*, the dorsal centra are opisthocoelous, the pleurocoels of dorsal centra have acute anterior and posterior margins, and the dorsoventral height of the neural arch is lower than the height of the dorsal centrum in *Chuanjiesaurus anaensis*. In contrast to *Xinjiangtitan shanshanesis, Chuanjiesaurus anaensis* is apparently different from its knob-like fused neural spines, a thin prespinal lamina between the spinoprezygapophyseal laminae and V-shaped shelf-like hyposphene in posterior dorsal vertebrae. There are three laminae supporting the infrahyposphenal cavity of the dorsal neural arch in *Chuanjiesaurus anaensis*, while there is no cavity beneath the hyposphene in *Xinjiangtitan shanshanesis*. Furthermore, the SPOLs are relatively thick single plates and no bifurcated M. SPOL, A.SPOL, P.SPOL and bif.SPRL in *Chuanjiesaurus anaensis*.

Analong chuanjieensis

Analong chuanjieensis (Ren et al. 2020) was recovered from the base of the Chuanjie Formation, which is regarded to be Middle Jurassic (Bajocian) (Huang et al. 2015; Ren et al. 2020). Ren et al. (2020) considered it as the earliest branching of Mamenchisauridae. The holotype (LCD9701-1) has eight middle-posterior dorsal vertebrae, but most of them are partly preserved (Ren et al. 2020).

The length/posterior surface height ratios of the posterior dorsal centra in *Analong chuanjieensis* range from 0.67 to 0.83 (Ren et al. 2020), which differ from that in *Xinjiangtitan shanshanesis* (0.73 ~ 1.09). The height/the width of posterior surface in posterior centra of *Analong chuanjieensis* is about 1.6, which is larger than that in *Xinjiangtitan shanshanesis* (about 0.75). Unlike the single deep pleurocoel without septa in *Xinjiangtitan shanshanesis*, the lateral pneumatic fossa of centra is divided into two small elliptical fossae by septa in *Analong chuanjieensis*. In *Analong chuanjieensis*, the hyposphene-hypantrum system is weakly developed under the postzygapophyses as 'V'-shaped in posterior vertebrae, whereas the system is absent in posterior dorsal vertebrae (dorsals 9–12) of *Xinjiangtitan shanshanesis*. The dorsal neural spines of posterior dorsals in *Analong chuanjieensis* present as knob-shaped, but that of *Xinjiangtitan shanshanesis* presents as rectangle-shaped, wider transversely than long with a weakly developed medial tubercle.

Discussion

Our detailed description and morphological comparison suggest that *Xinjiangtitan shanshanesis* can be distinguished from all other relevant sauropods from the Middle-Late Jurassic of China. Zhang et al. (2020) proposed that cervical vertebrae of *Xinjiangtitan shanshanesis* are similar to *Qijianglong guokr*, especially in the posteriorly extended epipophysis, but comparative anatomical data of dorsal vertebrae indicate that there are plenty of differences between the two taxa. Furthermore, through comparing the vertebrae of *Hudiesaurus sinojapanorum*, we found that there are many similarities in the last cervical vertebra and the first two dorsal vertebrae of *Xinjiangtitan shanshanesis*, such as two accessory laminae subdivided the SDF, pleurocoel subdivided by an oblique lamina as that in cervical 18, small coels on the dorsal surfaces of prezygapophyses as in cervical 18 and dorsals 1–2, the 'V' -shaped TPOL as in dorsal1. Interestingly, *Xinjiangtitan shanshanesis* shares the dorsally bifurcated M. SPDL in middle dorsal vertebrae, which was thought to be a unique autopomorphy of *Klamelisaurus gobiensis* (Moore et al. 2020). *Xinjiangtitan shanshanesis* shares the M. SPDL and the L. SPDL, however, the L. SPDL is not observed in *Klamelisaurus gobiensis*.

Similar to the condition of the cervical vertebrae (Zhang et al. 2020), the dorsal vertebrae of the *Xinjiangtitan shanshanesis* share

many features similar to other mamenchisaurid sauropods. However, *Xinjiangtitan shanshanesis* bears several unique features, some of which are similar to the more derived non-mamenchisaurid sauropods, for example, the middle dorsal vertebrae bear the M.SPOL and the L.SPOL, which are similar to the divided SPOL in *Apatosaurus* (Gilmore 1936; Upchurch et al. 2004); the M.SPOL and the L.SPOL define a shallow intralaminar SPOL-F, which is similar to the SPOL-F of posterior dorsal vertebrae in *Camarasaurus supremus* (Wilson et al. 2011: Fig. 9; Obsborn and Mook 1921), but differs from the SPOL-F in *Apatosaurus* (Gilmore 1936; Upchurch et al. 2004; Wilson et al. 2011: Fig. 12). We also note that the lamination of dorsal vertebrae in *Xinjiangtitan shanshanesis* is more developed and complicated than other members of Mamenchisauridae, for instance, two nearly parallel CPOLs in dorsal series.

Conclusion

Our redescription, comparison and phylogenetic analysis of *Xinjiangtitan shanshanesis* further indicate that it is a valid member of Mamenchisauridae, with possible close relationship to *Hudiesaurus* and *Mamenchisaurus*.

The redescription of *Xinjiangtitan* dorsal vertebrae provides additional information to help understand the dominant Late Jurassic sauropod lineage and the evolutionary history of sauropods in Eastern Asia. This study also suggests that there is a more complex diversity and evolutionary process of Mamenchisauridae happened than we thought before.

Abbreviation

Institutional abbreviations

SSV, Shanshan Geological Museum, Shanshan.

Anatomical abbreviations

In this work, descriptions of vertebral laminae and fossae follow the nomenclature of Wilson (1999), Wilson and Upchurch (2009), Wilson et al. (2011) and Wilson (2012). acdl (ACDL), anterior centrodiapophyseal lamina; acpl (ACPL), anterior centroparapophyseal lamina; a.r (A.R), accessory ridge; a.spdl (A.SPDL), anterior spinodiapophyseal laminae; bif.spdl (bif.SPDL), bifurcated spinodiapophyseal lamina; bif.m.spdl (bif.M.SPDL), bifurcated middle spinodiapophyseal lamina bif.SPRL, bifurcated spinoprezygapophyseal lamina; cap (CAP), capitulum; cdf (CDF), centrodiapophyseal fossa; cpaf (CPAF), centroparapophyseal fossa; cpof (CPOF), centropostzygapophyseal fossa; cpol (CPOL), centropostzygapophyseal lamina; cprf (CPRF), centroprezygapophyseal fossa; cprl (CPRL), centroprezygapophyseal lamina; Cv, cervical vertebra; D, dorsal vertebra; eprl (EPRL), epipophyseal-prezygapophyseal lamina; h.l (H.L), horizontal lamina; h.a.s (H.A.S), horizontal accessory strut; h.r (H.R), horizontal accessory ridge; l.cpol (L.CPOL), lateral centropostzygapophyseal lamina; l.sdf (L.SDF), lower spinodiapophyseal fossa; l.spol (L.SPOL), lateral spinopostzygapophyseal lamina; m.cpol (M.CPOL), medial centropostzygapophyseal lamina; m.spdl (M.SPDL), middle spinodiapophyseal lamina; m.spol (M.SPOL), medial spinopostzygapophyseal lamina; mp (MP), metapophysis; mt (MT), median tubercle; o.l (O.L), oblique lamina; o.r (O.R), oblique accessory ridge; pa (PA), parapophysis; pacdf (PACDF), parapophyseal centrodiapophyseal fossa; pacprf (PACPRF), parapophyseal centroprezygapophyseal fossa; pcdl (PCDL), posterior centrodiapophyseal lamina; pcpl (PCPL), posterior centroparapophyseal lamina; pf(PF), pneumatic fossa; pl(PL), pleurocoel; pml (PML), posterior midline lamina; pocdf (POCDF), postzygapophyseal centrodiapophyseal fossa; podl (PODL), postzygodiapophyseal lamina; poz (POZ), postzygapophysis; ppdl (PPDL), paradiapophyseal lamina; prcdf (PRCDF), prezygapophyseal centrodiapophyseal fossa; prdl (PRDL), prezygodiapophyseal lamina; prpl (PRPL), prezygoparapophyseal lamina; prz (PRZ), prezygapophysis; prz.p (PRZ.P), pits on dorsal surface of prezygapophysis; prpadf (PRPADF), prezygapophyseal paradiapophyseal fossa; p.spdl (P.SPDL) posterior spinodiapophyseal lamina; s (S), sacral vertebra; s.c (S.C), secondary crest; sdf (SDF), spinodiapophyseal fossa; sp (SP), neural spine; spdl (SPDL), spinodiapophyseal lamina; spof (SPOF), spinopostzygapophyseal fossa; spol (SPOL), spinopostzygapophyseal lamina; spol-f (SPOL-F), spinopostzygapophyseal lamina fossa; sprf (SPRF), spinoprezygapophyseal fossa; sprl (SPRL), spinoprezygapophyseal lamina; tlp (TLP), triangular lateral process; t.p (T.P), transverse precess; tprl (TPRL), intraprezygapophyseal lamina; tpol (TPOL), intrapostzygapophyseal lamina; tub (TUB), tuberculum; u.sdf (U.SDF), upper spinodiapophyseal fossa; v.r (V.R), vertical secondary ridge.

Acknowledgments

For their hospitality and access to specimens in their care, we thank the Shanshan Geological Museum. We wish to thank Gansu Sinian Dinosaur Culture Communication Co. Ltd. for their field assistance and the preparation of the specimen. We are grateful to Dr Lü Junchang, Wang YM, Yang JT, Li LF, Zhang QN and Ren XX for all of their assistance. Fieldwork funding was provided by the Rescue Excavation Project of Dinosaur Fossils in Shanshan, Xinjiang. HLY is supported by the Strategic Priority Research Program of the Chinese Academy of Sciences (XDB26000000) and the National Natural Science Foundation of China (Grants No. 42288201, 41872021 and 41472020).

Disclosure statement

No potential conflict of interest was reported by the author(s).

ORCID

Hai-Lu You http://orcid.org/0000-0003-2203-6461

References

Alexander RM. 1989.Dynamics of dinosaurs and other extinct giants. New York: Columbia University Press; p. 167.

Bonaparte JF. 1986. The early radiation and phylogenetic relationships of the Jurassic Sauropod dinosaurs, based on vertebral anatomy. In: Padian K, editor. The Beginning of the Age of Dinosaurs. Cambridge: Cambridge University Press; p. 247–258.

Cao YS, You HL. 2000. The jaw of *Datousaurus bashanensis* Dong and Tang,1984. Acta Palaeontologica Sinica. 39(3):391–395.

Dai H, Tan C, Xiong C, Ma QY, Li N, Yu HD, Wei ZY, Wang P, Jian Yi J, Wei GB, et al. 2022. New macronarian from the Middle Jurassic of Chongqing, China: phylogenetic and biogeographic implications for neosauropod dinosaur evolution. R Soc Open Sci. 9(11):220794. doi:10.1098/rsos.220794.

D'Emic MD. 2012. The early evolution of titanosauriform sauropod dinosaurs. Zool J Linn Soc. 166(3):624–671. doi:10.1111/j.1096-3642.2012.00853.x.

Dong ZM. 1990. Sauropoda from the Kelameili Region of the Junggar Basin, Xinjiang Autonomous Region. Vertebrata Palasiatica. 28:43–58.

Dong ZM. 1992. Dinosaurian Faunas of China. Beijing: China Ocean Press; p. 188.

Dong ZM. 1997. A gigantic sauropod (*Hudiesaurus sinojapanorum* gen. et sp. nov.) from the Turpan Basin, China. In: Dong ZM, editor. Sino-Japanese Silk Road Dinosaur Expedition. Beijing: China Ocean Press; p. 102–110.

Dong ZM, Tang ZL. 1984. Note on a new mid-Jurassic sauropod (*Datousaurus bashanensis* gen. et sp. nov.) from Sichuan basin, China. Certebrata Palasiatica. XXII(1):69–74. In Chinese.

Dong ZM, Zhou SW, Zhang YH. 1983. Dinosaurs from the Jurassic of Sichuan. Palaeontologica Sinica, Series C. 162:1–136.

Fang XS, Pang QQ, Lu LW, Zhang ZX, Pan SG, Wang YM, Li XK, Cheng ZW 2000. Lower, middle, and upper Jurassic subdivision in the Lufeng region, Yunnan Province. In: Editorial Committee of the Proceedings of the Third National Stratigraphical Congress of China. Beijing: Geological Publishing House; p. 208–214. [In Chinese].
Fang Y, Wu C, Guo Z, Hou K, Dong L, Wang L, Li L. 2015. Provenance of the southern Junggar Basin in the Jurassic: evidence from detrital zircon geochronology and depositional environments. Sedimentary Geology. 315 (1):47–63. doi:10.1016/j.sedgeo.2014.10.014.
Gilmore CW. 1936. Osteology of *Apatosaurus* with special reference to specimens in the Carnegie Museum. Memoirs of the Carnegie Museum. 11 (4):175–300. doi:10.5962/p.234849.
Goloboff PA, Catalano SA. 2016. TNT version 1.5, including a full implementation of phylogenetic morphometrics. Cladistics. 32(3):221–238. doi:10.1111/cla.12160.
Goloboff PA, Farris JS, Nixon KC. 2008. TNT, a free program for phylogenetic analysis. Cladistics. 24(5):1–13. doi:10.1111/j.1096-0031.2008.00217.x.
Harris JD. 2006a. The axial skeleton of the dinosaur *Suuwassea emilieae* (Sauropoda: Flagellicaudata) from the upper Jurassic Morrison Formation of Montana, USA. Palaeontology. 49(5):1091–1121. doi:10.1111/j.1475-4983.2006.00577.x.
Harris JD. 2006b. The significance of *Suuwassea emilieae* (Dinosauria: Sauropoda) for Flagellicaudatan intrarelationships and evolution. Journal of Systematic Paleontology. 4(2):185–198. doi:10.1017/S1477201906001805.
Hatcher JB. 1901. *Diplodocus* (Marsh): its osteology, taxonomy, and probable habits, with a restoration of the skeleton. Memoirs of the Carnegie Museum. 1(1):1–63. doi:10.5962/p.234818.
Hedrick BP, Dodson P. 2020. Paleobiology in the 21st century. The Anatomical Record. 303(4):645–648. doi:10.1002/ar.24384.
He XL, Li K, Cai KJ. 1988. Sauropod dinosaur (2) *Omeisaurus tianfuensis*. The middle Jurassic dinosaurian fauna from Dashanpu, Zigong, Sichuan 4. Chengdu: Sichuan Publishing House of Science and Technology; p. 1–143.
He XL, Yang SH, Cai KJ, Li K, Liu ZW. 1996. A new species of sauropod, *Mamenchisaurus anyuensis* sp. nov. Department of Land and Resources, State Development Planning Commission and Department of Science and Technology, Ministry of Geology and Mineral Resources. Papers on geosciences contributed to the 30th international geological congress. Beijing (China): China Economic Publishing House; p. 83–86.
Huang D. 2019. Jurassic integrative stratigraphy and timescale of China. Science China Earth Science. 62(1):227–259. doi:10.1007/s11430-017-9268-7.
Huang BC, Li YA, Fang XS, Sun DJ, Pang QQ, Cheng ZW, Li PX. 2015. Magnetostratigraphy of the Jurassic in Lufeng, central Yunnan. Regional Geology of China. 24:322–328.
Huang JD, You HL, Yang JT, Ren XX. 2014. A new sauropod dinosaur from the Middle Jurassic of Huangshan, Anhui Province. Vertebrata Palasiatica. 52:390–400.
Huene FV. 1932. Die Fossile Reptil-Ordnung Saurischia: ihre Entwicklung und Geschichte. Gebruder Borntraeger. Monographien zur Geologie und Palaeontologie. 4:1–361.
Jiang S, Li F, Peng GZ, Ye Y. 2011. A new species of Omeisaurus from the middle Jurassic of Zigong. Sichuan.Vertebrata PalAsiatica. 49(2):185–194.
Moore AJ, Mo JY, Clark JM. 2018. Cranial anatomy of *Bellusaurus sui* (Dinosauria: Eusauropoda) from the Middle-Late Jurassic Shishugou Formation of northwest China and a review of sauropod cranial ontogeny. In: Xu X, editor. PeerJ. 6(2):e4881. doi:10.7717/peerj.4881
Kuang XW. 2004. A new Sauropoda from Kaijiang dinosaur fauna in middle Jurassic beds of North-Eastern Sichuan. In: Sun JW, editor. Collection of the 90th anniversary of Tianjin Museum of Natural History. Tianjin: Tianjin Science and Technology Press; p. 40.
Li K. 1998. The sauropoda fossils and their stratigraphical distribution in China. Journal of Chengdu University of Technology. 25(1):53–60. In Chinese.
Li ZG 2012. The quantitative phylogenetic analysis of *Mamenchisaurus anyuensis*. (Master thesis, Chengdu University of Technology).
Li K, Liu J, Yang C, Hu F. 2011. Dinosaur assemblages from the Middle Jurassic Shaximiao Formation and Chuanjie Formation in the Sichuan-Yunnan Basin, China. Volumina Jurassica. 9:21–42.
Lü JC, Li TG, Zhong SM, Ji Q, Li SX. 2008. A New Mamenchisaurid Dinosaur from the Middle Jurassic of Yuanmou, Yunnan Province. Acta Geologica Sinica. 82:17–26.
Lü JC, SX LI, Ji Q, Wang GF, Zhang JH, Dong ZM. 2006. New Eusauropod dinosaur from Yuanmou of Yunnan Province, China. Acta Geologica Sinica: English Edition. 80(1):1–10. doi:10.1111/j.1755-6724.2006.tb00788.x.
Mannion PD, Upchurch P, Barnes RN, Mateus O. 2013. Osteology of the Late Jurassic Portuguese sauropod dinosaur *Lusotitan atalaiensis* (Macronaria) and the evolutionary history of basal titanosauriforms. Zool J Linn Soc. 168:98–206.
Mannion PD, Upchurch P, Jin X, Zheng W. 2019. New information on the Cretaceous sauropod dinosaurs of Zhejiang Province, China: impact on Laurasian titanosauriform phylogeny and biogeography. Royal Society Open Science. 6(8):191057. doi:10.1098/rsos.191057.
Mannion PD, Upchurch P, Mateus O, Barnes RN, Jones MEH. 2012. New information on the anatomy and systematic position of *Dinheirosaurus lourinhanensis* (Sauropoda: Diplodocoidea) from the late Jurassic of Portugal, with a review of European diplodocoids. Journal of Systematic Palaeontology. 10(3):521–551. doi:10.1080/14772019.2011.595432.
Marsh OC. 1878. Principal characters of American Jurassic dinosaurs (Part 1). American Journal of Science (Series. 3), 16(95):411–416. doi:10.2475/ajs.s3-16.95.411.
Martin J, Martin-Rolland V, Frey E. 1998. Not cranes or masts, but beams: the biomechanics of sauropod necks. Oryctos. 1:113–120.
McIntosh JS. 1990. Sauropoda (eds. Weishampel DB, Dodson P, Osmvólska H). Berkeley: University of California Press; p., 345–401.
Mo JY. 2013. Topics in Chinese Dinosaur Paleontology: *Bellusaurus sui*. Zhengzhou (China): Henan science and technology; p. 1–69. In Chinese
Moore A, Clark J, Xu X 2017. T1 - ABSTRACT: anatomy and systematic of *Klamelisaurus gobiensis*, a mamenchisaurid sauropod from the Middle-Late Jurassic Shishugou Formation of China. Program and Abstracts of Annual Meeting of the Society of Vertebrate Paleontology, Salt Lake City, Utah. 165–166. doi:10.13140/RG.2.2.14403.30245.
Moore AJ, Upchurch P, Barrett PM, Clark JM. 2020. Osteology of *Klamelisaurus gobiensis* (Dinosauria, Eusauropoda) and the evolutionary history of Middle–Late Jurassic Chinese sauropods. In: Xu X, editors. Journal of Systematic Palaeontology. 18(16):1299–1393. doi:10.1080/14772019.2020.1759706.
Osborn HF, Mook CC. 1921. *Camarasaurus, Amphicoelias*, and other sauropods of Cope. Memoirs of the American Museum of Natural History (New Series). 3:249–387.
Ouyang H. 1989. A new sauropod from Dashanpu, Zigong Co., Sichuan Province (*Abrosaurus dongpoensis* gen. et sp. nov.). Zigong Dinosaur Museum Newsletter. 2:10–14.
Ouyang H, Ye Y. 2002. The first mamenchisaurian skeleton with complete skull, *Mamenchisaurus youngi*. Chengdu: Sichuan Publishing House of Science and Technology; p. 1–111.
Owen R. 1842. Report on British Fossil Reptiles, Part II. Report of the British Association for the Advancement of Science. 11:60–204.
Paul GS. 2010. Euhelopids and mamenchisaurids. In: Paul Gregory S, editors. The Princeton field guide to dinosaurs (Vol. 178) (p. 320). Princeton: Princeton University Press.
Peng GZ, Ye Y, Gao YH, Shu CK, Jiang S. 2005. Jurassic dinosaur faunas in Zigong. Chengdu (China): Sichuan People's Publishing House, Chengdu; p. 236. In Chinese.
Pi LZ, Ouyang H, Ye Y. 1996. A new species of sauropod from Zigong, Sichuan: *Mamenchisaurus youngi*. editor. Department of Spatial Planning and Regional Economy. Beijing:China Economic Publishing House;87–91.
Ren XX, Huang JD, You HL. 2018. The second Mamenchisaurid dinosaur from the Middle Jurassic of Eastern China. Historical Biology. 32(5):602–610. doi:10.1080/08912963.2018.1515935.
Ren XX, JiangS, Wang XR, Peng GZ, Ye Y, King L, YouHL. 2022. Osteology of *Dashanpusaurus dongi* (Sauropoda: Macronaria) and new evolutionary evidence fromMiddle Jurassic Chinese sauropods. Journal of Systematic Palaeontology. 20: 1, 2132886, doi:10.1080/14772019.2022.2132886.
Ren XX, Sekiya T, Wang T, Yang ZW, You HL. 2020. A revision of the referred specimen of *Chuanjiesaurus anaensis* Fang et al. 2000: a new early branching mamenchisaurid sauropod from the middle Jurassic of China. Historical Biology. 2:1–16.
Russell DA, Zheng Z. 1993. A large mamenchisaurid from the Junggar Basin, Xinjiang, People Republic of China. Canadian Journal of Earth Sciences. 30 (10):2082–2095. doi:10.1139/e93-180.
Salgado LR, Coria A, Calvo JO. 1997. Evolution of titanosaurid sauropods. I: phylogenetic analysis based on the postcranial evidence. Ameghiniana. 34:3–32.
Seeley HG. 1887. On the classification of the fossil animals commonly named Dinosauria. Proceedings of the Royal Society of London. 43(1887–1888):165–171.
Sekiya T. 2011. Re-examination of *Chuanjiesaurus anaensis* (Dinosauria: sauropoda) from the middle Jurassic chuanjie formation, Lufeng County, Yunnan Province, southwest China. Memoir of the Fukui Prefectural Dinosaur Museum. 10:1–54.
Seymour RS, Lillywhite HB. 2000. Hearts, neck posture and metabolic intensity of sauropod dinosaurs. Proceedings of the Royal Society B-Biological Sciences. 267(1455):1883–1887.
Tang F, Jing XS, Kang XM, Zhang GJ. 2001. *Omeisaurus maoianus*: a complete Sauropod from Jingyuan, Sichuan. Beijing (China): China Ocean Press; p. 1–128.
Tan C, Xiao M, Dai H, Hu XF, Li N, Ma QY, Zhao YW, Yu DH, Xiong C, Peng GZ, Jiang S, Ren XX, You, HL. 2020. A new species of *Omeisaurus* (Dinosauria: Sauropoda) from the Middle Jurassic of Yunyang, Chongqing, China. Historical Biology, 33(9):1817–1829.

Upchurch P. 1995. The evolutionary history of sauropod dinosaurs. Philosophical Transactions of the Royal Society of London, Series B. 349:365–390.
Upchurch P. 1998. The phylogenetic relationships of sauropod dinosaurs. Zool J Linn Soc. 124(1):43–103. doi:10.1111/j.1096-3642.1998.tb00569.x.
Upchurch P, Mannion PD, Xu X, Barrett PM. 2021. Re-assessment of the Late Jurassic eusauropod dinosaur *Hudiesaurus sinojapanorum* Dong, 1997, from the Turpan Basin, China, and the evolution of hyper-robust antebrachia in sauropods. Journal of Vertebrate Paleontology. 41(4). doi:10.1080/02724634.2021.1994414.
Upchurch P, Tomida Y, Barrett PM. 2004. A new specimen of *Apatosaurus ajax* (Sauropoda: Diplodocidae) from the Morrison Formation (Upper Jurassic) of Wyoming USA. National Science Museum Monographs. 26:1–108.
Vidal D, Mocho P, Aberasturi A, Sanz JL, Ortega F. 2020. High browsing skeletal adaptations in spinophorosaurus reveal an evolutionary innovation in sauropod dinosaurs. Scientific Reports. 10(1). doi:10.1038/s41598-020-63439-0.
Wilson JA. 1999. A nomenclature for vertebral laminae in sauropod dinosaurs and other saurischian dinosaurs. Journal of Vertebrate Paleontology. 19(4):639–653. doi:10.1080/02724634.1999.10011178.
Wilson JA. 2002. Sauropod dinosaur phylogeny: critique and cladistic analysis. Zool J Linn Soc. 136(2):215–275. doi:10.1046/j.1096-3642.2002.00029.x.
Wilson JA. 2012. New vertebral laminae and patterns of serial variation in vertebral laminae of Sauropod Dinosaurs. Contributions from the Museum of Paleontology, University of Michigan. 32(7):91–110.
Wilson JA, D'Emic MD, Ikejiri T, Moacdieh EM, Whitlock JA, Farke A. 2011. A nomenclature for vertebral fossae in sauropod dinosaurs and other saurischian dinosaurs. PLoS One. 6(2):e17114. doi:10.1371/journal.pone.0017114.
Wilson JA, Sereno PC. 1998. Early evolution and higher-level phylogeny of sauropod dinosaurs. Memoir of the Society of Vertebrate Paleontology. 5:1–79. doi:10.2307/3889325.
Wilson JA, Upchurch P. 2009. Redescription and reassessment of the phylogenetic affinities of *Euhelopus zdanskyi* (Dinosauria: Sauropoda) from the early cretaceous of China. Journal of Systematic Palaeontology. 7(2):199–239. doi:10.1017/S1477201908002691.
Wiman C. 1929. Die Kriede-dinosaurier aus Shantung. Palaeontologia Sinica Series C. 6:1–67.
Wings O, Schwarz-Wings D, Fowler DW. 2011. New sauropod material from the Late Jurassic part of the Shishugou Formation (Junggar Basin, Xinjiang, NW China). Neues Jahrbuch für Geologie und Paleontologie - Abhandlungen. 262(2):129–150. doi:10.1127/0077-7749/2011/0183.
Wu WH, Zhou CF, Oliver W, Sekiya T, Dong ZM. 2013. A new gigantic sauropod dinosaur from the middle Jurassic of Shanshan. Xinjiang.Global Geology. 32: 437–446. [In Chinese].
Xing LD, Miyashita T, Currie PJ, You HL, Zhang JP, Dong ZM. 2015b. A new basal eusauropod from the Middle Jurassic of Yunnan, China, and faunal compositions and transitions of Asian sauropodomorph dinosaurs. Acta Palaeontologica Polonica. 60(1):145–154. doi:10.4202/app.2012.0151.
Xing LD, Miyashita T, Zhang JP, Li DQ, Ye Y, Sekiya T, Wang FP, Currie PJ. 2015a. A new sauropod dinosaur from the late Jurassic of China and the diversity, distribution, and relationships of mamenchisaurids. Journal of Vertebrate Paleontology. 35(1):e889701. doi:10.1080/02724634.2014.889701.
Xu X, Upchurch P, Mannion PD, Barrett PM, Regalado-Fernandez OR, Mo JY, Ma JF, Há L. 2018. A new Middle Jurassic diplodocoid suggests an earlier dispersal and diversification of sauropod dinosaurs. Nat Commun. 9(1):2700. doi:10.1038/s41467-018-05128-1.
Yates AM. 2007. The first complete skull of the Triassic dinosaur Melanorosaurus Haughton (Sauropodomorpha: Anchisauria). Special Papers in Palaeontology. 77:9–55.
Ye Y, Gao YH, Jiang S. 2005. A new genus of sauropod from Zigong, Sichuan. Vertebrata Palasiatica. 43(3):175–181.
Young CC. 1937. A new dinosaurian from Sinkiang. Palaeontologia Sinica, Series C. 2:1–25.
Young CC. 1939. On a new Sauropoda, with notes on other fragmentary reptiles from Szechuan. Bulletin of the Geological Society of China. 19:279–315. doi:10.1111/j.1755-6724.1939.mp19003005.x.
Young CC. 1954. On a new sauropod from Yiping, Szechuan, China. Acta Paleontologica Sinica. 2:355–369.
Young CC. 1958. New sauropod dinosaurs from China. Vertebrata Pal Asiatica. 2:1–29.
Young CC, Chao XJ. 1972. *Mamenchisaurus hochuanensis* sp. nov. Institute of Vertebrate Paleontology and Paleoanthropology Monographs (Series A) . 8: 1–30. In Chinese
Zhang YH. 1988. Shunosaurus lii. The Middle Jurassic Dinosaur Fauna from Dashanpu. Zigong (Sichuan): Sauropod Dinosaurs.
Zhang YG, Li JJ. 2001. Supplementary research of *Mamenchisaurus jingyanensis* from new specimens. Journal of Zhejiang University. 59: 17–21. In Chinese.
Zhang XQ, Li DQ, Xie Y, You HL. 2020. Redescription of the cervical vertebrae of the mamenchisaurid sauropod *Xinjiangtitan shanshanesis* Wu et al. 2013. Historical Biology. 32(6):802–822. doi:10.1080/08912963.2018.1539970.
Zhang YH, Li K, Zeng QH. 1998. A new species of sauropod from the Late Jurassic of the Sichuan Basin (*Mamenchisaurus jingyanensis* sp. nov.). Journal of Chengdu University of Technology. 25(1):61–70.
Zhang YH, Yang DH, Peng GZ. 1984. New materials of *Shunosaurus* from the Middle Jurassic of Dashanpu, Zigong, Sichuan. Journal of the Chengdu College of Geology. 2(Supplement):1–12.
Zhao XJ. 1993. A new mid-Jurassic sauropod (*Klamelisaurus gobiensis* gen.et sp. nov.) from Xinjiang China. Vertebrata PalAsiatica. 31(2):132–138. In Chinese.